IMPACT OF THE MICROSTRUCTURE OF PRECIPITATION AND HYDROMETEORS ON MULTI-FREQUENCY RADAR OBSERVATIONS

Jussi Leinonen

Department of Applied Physics
School of Science
Aalto University
Espoo, Finland

Doctoral dissertation for the degree of Doctor of Science in Techology to be presented with due permission of the School of Science for public examination and debate in Auditorium L at the Aalto University School of Science (Espoo, Finland) on the 17th of May 2013 at 12 noon.

![Finnish Meteorological Institute logo] FINNISH METEOROLOGICAL INSTITUTE

Author
Jussi Leinonen

Title

Impact of the microstructure of precipitation and hydrometeors on multi-frequency radar observations

Abstract

Continuous observations are needed to monitor and predict the state of the changing Earth system. These observations must be global, and therefore areas with poor or no infrastructure also have to be covered by them. Remote sensing systems, especially those based on satellites, are a practically achievable way to make measurements also in such remote areas.

The hydrological cycle is a critical part of the atmosphere-ocean system. It is monitored remotely by many satellites, but the need for new technologies to improve the accuracy of the measurements is widely recognized. Precipitation and cloud radars appear to be promising tools, but have so far been operated in only two satellites. Typically, space-based radars use shorter wavelengths than most ground-based weather radars. This complicates the problem of modeling the radar scattering, whose nature depends on the size of the targets relative to the wavelength. Understanding the radar scattering at short wavelengths is particularly important for multi-frequency radars, which are used to infer additional information about their targets from the difference of signals of different frequencies, and thus originating from different scattering processes. These radars require that one of the wavelengths be of the order of the typical target hydrometeor size or shorter.

The Arctic and the Antarctic, which are particularly significant among Earth's remote areas because of their sensitivity to climate change, present specific challenges and opportunities for spaceborne radars. Compared to regions closer to the equator, the typically light precipitation rate, small size of precipitating particles and common occurrence of snowfall in these areas require radars to have higher sensitivity. Because of the small hydrometeor size, respectively shorter wavelengths are needed there to use a multi-frequency system. On the other hand, these factors also mean that signal attenuation by the hydrometeors is usually fairly weak. This increases the suitability of short-wavelength radars, whose signal is attenuated more strongly in the atmosphere than those with longer wavelengths.

This thesis is also concerned with the complex shapes of snowflakes, which make the interpretation of the scattered signals more difficult. It has previously been a common practice in radar scattering computations to simplify the particle structure to an equivalent analytical model, but it turns out that such models are often not consistently usable at high frequencies, above roughly 30–90 GHz depending on the snowflake size. Instead, the shape model should describe also the microstructure of the snowflakes. An autocorrelation-based particle model is suggested herein as an alternative that can adequately account for that structure and yet remain simple enough to be suitable for the interpretation of radar observations.

Nimike
Sateen ja hydrometeorien rakenteen vaikutus monitaajuustutkahavaintoihin

Tiivistelmä

Maan ilmakehän muuttuvan tilan valvontaan ja ennustamiseen tarvitaan jatkuvaa havainnointia. Havaintoja täytyy tehdä kaikkialla maapallolla, ja siksi niiden täytyy kattaa myös alueet, joilla on huono tai olematon infrastruktuuri. Kaukokartoituslaitteilla, varsinkin satelliiteihin asennetuilla, voidaan tehdä mittauksia käytännöllisesti myös näillä syrjäisillä alueilla.

Hydrologinen kierto on elintärkeä osa ilmakehän ja merten muodostamaa järjestelmää. Sitä valvotaan kaukokartoituslaitteilla useista satelliiteista käsin, mutta mittausten tarkkuuden parantamiseen tarvitaan uutta teknologiaa. Sade- ja pilvitutkat vaikuttavat lupaavilta mittalaitteilta, mutta näitä on tähän asti käytetty vain kahdessa satelliitissa. Satelliittitutkat käyttävät yleensä lyhyempiä aallonpituuksia kuin maan pinnalle asennetut säätutkat. Tämä monimutkaistaa tutkasironnan mallinnusta, sillä sironnan luonne riippuu mittauskohteiden koon ja aallonpituuden välisestä suhteesta. Tutkasironnan ymmärtäminen lyhyillä aallonpituuksilla on erityisen tärkeää monitaajuustutkille, jotka saavat mittauskohteista lisää tietoa tulkitsemalla eri taajuuksilla mitattujen, ja siten erilaisista sirontaprosesseista peräisin olevien signaalien eroja. Näissä tutkissa vähintään yhden aallonpituuksista on oltava tyypillisen hydrometeorin kokoluokkaa tai lyhyempi.

Arktiset ja antarktiset alueet, jotka ovat merkittäviä syrjäisiä alueita johtuen niiden herkkyydestä ilmastonmuutokselle, asettavat omanlaisensa haasteet ja mahdollisuudet satelliittitutkille. Verrattuna päiväntasaajaa läheisempiin alueisiin, näiden alueiden tyypillisesti heikko sade, hydrometeorien pieni koko ja lumisateen yleisyys vaativat tutkilta suurempaa herkkyyttä. Monen taajuuden tutkajärjestelmän käyttämiseen näillä alueilla tarvitaan kohteiden pienemmän koon vuoksi vastaavasti lyhyempiä aallonpituuksia. Toisaalta näistä syistä myös tutkasignaalin vaimeneminen näillä alueilla on yleensä melko heikkoa. Tämä parantaa lyhyiden aallonpituuksien tutkien käytettävyyttä, sillä näiden tavallinen heikkous on, että signaali vaimenee voimakkaammin kuin pidemmillä aallonpituuksilla.

Tässä väitöskirjassa käsitellään myös lumihiutaleiden monimutkaista muotoa, joka tekee havaintojen tulkitsemisesta hankalampaa. Tavallisesti tutkasirontaa laskettaessa on ollut tapana yksinkertaistaa kohdehiukkasen rakenne vastaavaan analyyttiseen malliin, mutta osoittautuu, että tällaisia malleja ei usein voida käyttää yksiselitteisellä tavalla korkeilla, lumihiutaleiden koosta riippuen yli 30–90 GHz, taajuuksilla. Hiukkasmallin tulisi sen sijaan kuvata myös lumihiutaleiden rakennetta. Autokorrelaatioon perustuvaa hiukkasmallia ehdotetaan tässä väitöskirjassa vaihtoehdoksi, joka ottaa rakenteen riittävällä tavalla huomioon ja on kuitenkin riittävän yksinkertainen käytettäväksi tutkahavaintojen tulkintaan.

Preface

The research leading to this thesis was performed during the years 2009–2013 at the Earth Observation unit of the Finnish Meteorological Institute. The work was further supported by the Academy of Finland, by the Aalto University, and by my colleagues at the University of Helsinki. Such a scholarly tangle involves simply too many people for their names to fit on this page. Instead, I begin with thanking my wife Jonna, who I met shortly before finishing my master's degree and who has been by my side for the whole process, as well as my mother Minna and my father Esa, on whose knee I sat for hours at a time at the age of six, when he worked on his thesis.

My biggest professional debt of gratitude is that to my co-authors: Dmitri, Chandra, Jarkko, Jani, Timo, Matti, Walt, Stefan, Simone and Chris. I would like to mention three of them in particular. Firstly, Dr. Timo Nousiainen, who agreed to be my advisor and took me under his guidance in his research group. Secondly, Dr. Dmitri Moisseev, who mentored me, was closely involved in each of my research projects since the beginning of our co-operation in 2009, and had the thankless task of being my *de facto* second advisor without official recognition as such. Thirdly, Dr. Jani Tyynelä, who spent countless hours with me enthusiastically discussing new ideas and encouraged me to focus on the interesting, important problems regardless of their (real or perceived) difficulty.

Also vital for the completion of this thesis were Prof. Risto Nieminen, my supervising professor at the Aalto University, and Dr. Ari-Matti Harri of the Finnish Meteorological Institute. It was under Ari-Matti that I had the chance to begin my career in atmospheric science already in the summer of 2005, and he had enough faith in me to accept me as a graduate researcher at the Radar and Space Technology group. Furthermore, Dr. Alessandro Battaglia of the University of Leicester and Prof. Johannes Verlinde of Pennsylvania State University pre-examined this thesis and gave helpful comments for improving it.

There are others who contributed to the work presented here in different ways — be it ideas, inspiration or enlightenment — and to whom I would like to extend my appreciation (and, in some cases, apologies). The colleagues I shared an office with, as well as everyone I had the opportunity to meet in Timo's graduate student group, were particularly important in this regard. For their advice and insight, I would also like to thank the radar experts at FMI, especially Dr. Elena Saltikoff, Jarmo Koistinen and Timo Kuitunen.

Finally, *to absent friends, lost loves, old gods, and the season of mists*.

Helsinki, April 2013

Jussi Leinonen

Contents

Original publications

I Leinonen, J., D. Moisseev, V. Chandrasekar, and J. Koskinen (2011), Mapping radar reflectivity values of snowfall between frequency bands, *IEEE Trans. Geosci. Remote Sens.*, *49*(8), 3047–3058, doi:10.1109/TGRS.2011.2117432.

Paper I presents mapping methods that can be used, when observing snowfall, to derive the radar reflectivity at one frequency band from the reflectivity at one or two other bands. The reflectivity mappings are derived by computing the backscattering properties of snowflakes for various densities and particle size distributions. It is concluded that the error of the reflectivity estimate can be greatly reduced by using an algorithm that combines the available information from two different frequencies. The mapping algorithm is tested using combined data from CloudSat and a ground radar as well as from the Wakasa Bay experiment. The author of this thesis performed the majority of the work of developing the algorithms and analyzing the testing data, as well as writing the article.

II Tyynelä, J., J. Leinonen, D. Moisseev, and T. Nousiainen (2011), Radar backscattering from snowflakes: comparison of fractal, aggregate and soft-spheroid models, *J. Atmos. Oceanic Technol.*, *28*, 1365–1372, doi:710.1175/JTECH-D-11-00004.1.

Paper II examines the effect of different snowflake models on the computed backscattering cross sections. Fractal, aggregate and spheroidal snowflakes of various sizes are considered. It is found that the spheroidal models can underestimate the backscattering cross section, at the worst case (large size and high frequency) by as much as two orders of magnitude. For smaller particles and lower frequencies, the backscattering cross sections computed from the spheroidal models are consistent with those from the fractal and aggregate models. The author performed the T-matrix scattering computations used for the spheroids and participated in the interpretation of the results.

III Leinonen, J., D. Moisseev, M. Leskinen, and W. Petersen (2012a), A climatology of disdrometer measurements of rainfall in Finland over five years with implications for global radar observations, *J. Appl. Meteor. Climatol.*, *51*, 392–404, doi:10.1175/JAMC-D-11-056.1.

Paper III analyzes the disdrometer observations of rainfall gathered from Järvenpää, Finland, during the period 2006–2010. Drop size distributions are derived from the data, and the corresponding radar properties are computed at various frequency bands. Statistics of the drop size distribution and radar parameters are presented. It is shown that the local climate is characterized by light rain and small drops, which can pose a challenge for the detection and measurement of rain by radars, especially space-based ones. The author's

role was to perform the analysis of the data and to write most of the article.

IV Leinonen, J., S. Kneifel, D. Moisseev, J. Tyynelä, S. Tanelli, and T. Nousiainen (2012b), Nonspheroidal behavior in millimeter-wavelength radar observations of snowfall, *J. Geophys. Res.*, *117*, D18205, doi:10.1029/2012JD017680.

Paper IV derives from earlier work that showed, using modeling, that different snowflake models can be distinguished by using three frequencies simultaneously. This method is subjected to an experimental test by applying it on results from the Wakasa Bay experiment. The triple-frequency behavior of the data is compared to that of various snowflake models. It is shown that in some cases, spheroidal models cannot explain the observed data with any realistic set of free parameters, and that the data is more consistent with the DDA results based on detailed aggregate snowflake models. The author performed the processing and analysis of the Wakasa Bay experiment data, and wrote the majority of the article text.

V Tyynelä, J., J. Leinonen, C. Westbrook, D. Moisseev, and T. Nousiainen (2013), Applicability of the Rayleigh-Gans approximation for scattering by snowflakes at microwave frequencies in vertical incidence, *J. Geophys. Res.*, *118*, doi:10.1002/jgrd.50167.

Paper V compares the scattering properties of snowflakes derived using the discrete dipole approximation (DDA) and the Rayleigh–Gans approximation (RGA). It is concluded that in snowflake scattering modeling, RGA can usually be used in place of the more accurate but also much more complicated and computationally expensive DDA, with only minor errors. Linear corrections are suggested to compensate for the bias of RGA. The author took part in the analysis of the results and contributed to the writing of the article.

VI Leinonen, J., D. Moisseev, and T. Nousiainen (2013), Linking snowflake microstructure to multi-frequency radar observations, *J. Geophys. Res.*, *118*, doi:10.1002/jgrd.50163.

Paper VI draws from earlier research on the physics of scattering by aggregate particles to formulate an autocorrelation-based description of snowflake structure. Combined with the Rayleigh–Gans scattering theory, this description can be used to derive the characteristics of the backscattering cross section as a function of frequency. It is suggested that snowflake models should be based on the autocorrelation rather than the average particle mass distribution. For the model developed in this paper, it is shown that the mass distribution-based shape model is a low-frequency approximation of the corresponding autocorrelation-based model. The author contributed a major part of the effort in deriving and testing the method, and wrote most of the article text.

1 Introduction

Precipitation is essential for human civilization, and yet it has been identified as one of the key uncertainties in the current understanding of the atmosphere-ocean system of the Earth [*Randall et al.*, 2007]. Besides moving water from the oceans to the continents as part of the hydrological cycle, precipitation also plays a significant role in transferring energy in the atmosphere [e.g. *Stephens et al.*, 2012]. Thus, global observations of precipitation are vital in the monitoring of the Earth system, and due to their wide coverage, remote sensing systems have become irreplaceable assets in the measurement of rain and snow.

Meteorological observations are scarce in the the Arctic and the Antarctic, deserts, oceans and other sparsely inhabited areas of the Earth. Due to the lack of infrastructure, in these areas measurements cannot usually be made at the site directly affected by the weather, leading to a lack of coverage. The conditions at these areas nevertheless affect the weather patterns experienced by more populous regions, and thus this data gap presents a concrete uncertainty for the understanding and, more tangibly, prediction of weather and climate at the midlatitudes. Furthermore, the nearly uninhabited high latitudes are the areas most severely affected by the ongoing changes in the Earth's climate [*Lemke et al.*, 2007].

The shortage of *in situ* observations in areas without extensive observational infrastructure has led to the introduction of meteorological remote sensing systems on the Earth's surface, in the air and in space. Remote sensing allows one to cover large areas of the globe with instruments that are installed far from each other. Ground-based remote sensing systems — whose range is limited by the curvature of the Earth — can observe the surface from a distance of many kilometers, and the atmosphere from up to hundreds of kilometers away. Of ground-based precipitation remote sensing systems, radars are the most commonly employed. They transmit pulses of electromagnetic radiation (typically microwaves with a frequency of 1–100 GHz), and measure the power and the delay of the returning signal, resolving both the intensity and the location of the target. This is in contrast to radiometers that passively measure the radiation emitted by hydrometeors. Nowadays, most highly developed areas are covered by networks of weather radars. However, their coverage is still limited to areas where the local infrastructure (the availability of electricity, telecommunications etc.) supports their deployment. Much greater flexibility is offered by moving airborne and spaceborne observation platforms. Satellite-based measurements, in particular, have become irreplaceable for observing the remote regions despite the expense of building and launching spacecraft.

The first radar-equipped spacecraft dedicated to measurements of rainfall, the Tropical Rainfall Measuring Mission (TRMM) operated by the National Aeronautics and Space Administration (NASA) of the United States, was launched in 1997 [*Kummerow et al.*, 2000]. TRMM operates a radar at 13.8 GHz (K_u-band) and a radiometer at 10.65 GHz, 19.35 GHz, 21.3 GHz, 37.0 GHz

and 85.5 GHz [*Kummerow et al.*, 1998; *Kozu et al.*, 2001]. It is still operational 15 years after launch. A somewhat different approach to space-based precipitation measurement was adopted for CloudSat, which observes clouds and precipitation using a 94-GHz (W-band) radar [*Stephens et al.*, 2002; *Tanelli et al.*, 2008]. Also differently from the tropical orbit of TRMM with an orbital inclination of 35°, CloudSat is on a near-polar orbit in the A-Train constellation at 98.2° inclination [*Stephens et al.*, 2008]. Because of its good coverage of high latitudes and the much greater sensitivity of its radar as compared with that of TRMM, CloudSat has been found suitable for measuring precipitation, especially snow, besides its primary function of observing clouds [e.g. *Ellis et al.*, 2009; *Haynes et al.*, 2009].

Two other spacecraft equipped with precipitation radars are currently under development. The Global Precipitation Measurement (GPM) core satellite is being prepared for a 2014 launch by NASA and the Japanese Aerospace Exploration Agency (JAXA) [*Iguchi et al.*, 2002; *Smith et al.*, 2007], and will include an upgraded version of the TRMM radar. This new instrument is known as the Dual-frequency Precipitation Radar (DPR), and operates at 13.6 GHz (K_u band) and 35.5 GHz (K_a band), with the goal of improving rain retrieval accuracy over TRMM [*Satoh et al.*, 2004]. The radiometer, GPM Microwave Imager (GMI), is likewise an improvement over that used in TRMM, with channels at 10.65 GHz, 18.7 GHz, 23.8 GHz, 36.5 GHz, 89 GHz, 166 GHz and 183.3 GHz [*Newell et al.*, 2010]. The other confirmed upcoming satellite is EarthCARE, developed by the European Space Agency (ESA) and JAXA, which uses a W-band radar similar to that of Cloud-Sat together with a lidar, multi-spectral imager and a broadband radiometer [*Hélière et al.*, 2007]. Various space agencies have also proposed other space missions that use precipitation radars, such as the NASA Aerosol/Clouds/Ecosystem (ACE) mission [*Tanelli et al.*, 2009] and the Polar Precipitation Mission concept [*Joe et al.*, 2010] that was proposed for ESA Earth Explorer 8.

The inherent difficulty of all remote sensing systems, including radars, is in the interpretation of the indirect measurements. The problem of interpretation of a remote observation is twofold. Firstly, one must understand how the observation is affected by the desired physical quantities as well as other, unwanted sources; this is called the *forward model*. Secondly, one needs to deduce the quantities, given the observation. Such inference tasks are called *inverse problems* and are common in indirect physical measurements. Typically, the forward process is such that the measurement does not convey complete information about the target, and thus assumptions about the nature of the target are required in order to solve the inverse problem. Radar measurements of precipitation are classical inverse problems, as they only produce a few measurable quantities from a very large number of hydrometeors. Regardless of this, radars can be used to determine the rainfall intensity with an error less than 25% using modern dual-polarization techniques and retrieval algorithms [*Illingworth*, 2004; *Wang and Chandrasekar*, 2010]. The forward model of radar observations must account for the transmission and reception of the pulses by the radar, their propagation in the atmosphere and the interaction of the electromagnetic radiation with the targets. The transmitter and the receiver can be controlled and calibrated, and the propagation is well understood (although it may be uncertain in cases in which the atmospheric temperature profile is unusual). Thus, the principal uncertainty of the forward model is arguably in the interaction, that is, the scattering and absorption of radiation, by the hydrometeors. Solving the inverse problem, then, requires one to infer the nature of the scatterers from the scattered radiation using knowledge about the scattering process.

The nature of precipitation at the high latitudes presents additional challenges to solving the inverse problem of retrieving the precipitation intensity from radar signals. The lower amount of available solar energy, as compared to lower latitudes, leads to a lower average intensity of precipitation, despite its fairly high occurrence in some areas, and thus places more stringent requirements on the sensitivity of radars. Furthermore, snow is common in these regions during the winter [e.g. *Heino and Hellsten*, 1983, for the statistics of Finland], giving rise to several complications. Due to the electromagnetic properties of ice, the radar echoes from falling snow are weaker than those from rain, and thus snow is more difficult to detect. The large variety in the shapes and densities of snowflakes also add complexity to the retrievals as opposed to the relatively well determined shape of raindrops as a function of size. Melting snow is even more challenging to measure because of the presence of water in both liquid and solid forms; it is also known to attenuate radar signals, which can be problematic for ground-based radar measurements when the $0\,°C$ isotherm is at ground level (*Pohjola and Koistinen* [2002] note that in Finland, this happens in approximately 5% of precipitation cases) and thus near-horizontal radar beams travel long distances through wet snow. Even when the melting layer is above ground level, it is often low, which interferes with the operation of space-based radars that cannot resolve the signal close to the ground due to the surface radar echo that overwhelms any nearby precipitation signals. Identifying the precipitation type is in itself nontrivial, and much research effort has been focused on this task [e.g. *Straka et al.*, 2000; *Lim et al.*, 2005].

The objective of this thesis has been to examine the use of multi-frequency radars to observe precipitation, particularly snow and light rain at the high latitudes. Specific focal points of the studies have been to characterize the effects of snowflake shape models in the interpretation of multi-frequency observations of snowfall, as well as the special considerations presented by high-latitude climates to multi-frequency precipitation observations. The goal or the research was to develop effective methods to overcome or alleviate the challenges presented by these factors.

The topic of multi-frequency radars has been treated with emphasis on spaceborne radars, particularly those on board the CloudSat and GPM satellites. This focus was motivated by the role of Finland as a GPM ground validation partner. Accordingly, several of the papers contain results and conclusions concerning the performance of satellite precipitation radars in high-latitude conditions. Besides spaceborne radar missions, the results can be applied to ground based multi-frequency radars such as those at the ARM sites [*Stokes and Schwartz*, 1994]. Spaceborne radars tend to use higher operating frequencies than ground-based radars, the wavelengths of the former being of the order of millimeters, the typical size of raindrops and snowflakes. Hence, major effort was also put into improving the understanding of scattering of millimeter-wave radiation by snowflakes (the corresponding problem for raindrops being already relatively well understood).

The present, introductory part of this thesis is organized as follows. In chapter 2, an overview is given of different computational scattering methods that are used to compute the radar signal from hydrometeors. Chapter 3 describes the basics of the microphysics and evolution of hydrometeors, and chapter 4 summarizes the principles and commonly used methods of measuring their properties. Chapter 5 introduces the particle (in particular, snowflake) shape models used to model the scattering from hydrometeors and to interpret remote measurements. Chapter 6 discusses the results and their implications in detail, and chapter 7 summarizes the findings and concludes the introductory part.

2 Scattering models

The physical properties of atmospheric hydrometeors can be measured with radar only if the scattering of microwaves from them is well understood, as this is what enables one to interpret the measurements. The modeling of radar scattering by hydrometeors is conceptually identical to many other problems in electromagnetic scattering (e.g. the scattering of visible light from nanometer- to micrometer-sized particles), as the the type of the problem depends mainly on the size of the particle relative to the wavelength of the radiation. The *size parameter x* of a particle is defined as $x = 2\pi r/\lambda = kr$, where $k = 2\pi/\lambda$ is the wavenumber and λ is the wavelength; x is typically used as the measure of the particle size in a scattering setting.

The formal solution of a scattering problem is given by the amplitude scattering matrix **S** that relates the incident electric field $\mathbf{E}^{\text{inc}}$ to the scattered field $\mathbf{E}^{\text{sca}}$. Using the notation of *Bringi and Chandrasekar* [2001] that is commonly used with weather radars,

$$\begin{bmatrix} E_{\text{h}}^{\text{sca}} \\ E_{\text{v}}^{\text{sca}} \end{bmatrix} = \frac{\exp(-ikr)}{r} \mathbf{S} \begin{bmatrix} E_{\text{h}}^{\text{inc}} \\ E_{\text{v}}^{\text{inc}} \end{bmatrix}, \tag{2.1}$$

where r is the distance and $i = \sqrt{-1}$ is the imaginary unit, and the subscripts h and v denote horizontal and vertical polarizations, respectively. The amplitude scattering matrix

$$\mathbf{S} = \begin{bmatrix} S_{\text{hh}} & S_{\text{hv}} \\ S_{\text{vh}} & S_{\text{vv}} \end{bmatrix} \tag{2.2}$$

is, in general, dependent on the directions of the incident and scattered radiation. It contains all information that is conveyed by the scattered waves about the scattering particle. The scattering quantities of interest can be computed from **S**; for example, the backscattering cross section needed in (4.2) is given by

$$\sigma_{\text{h}} = 4\pi |S_{\text{hh}}(\pi)|^2 \tag{2.3}$$

$$\sigma_{\text{v}} = 4\pi |S_{\text{vv}}(\pi)|^2 \tag{2.4}$$

where $|S_{\text{hh,vv}}(\pi)|$ denotes scattering in the exact opposite direction from the incident direction (in other words, at a scattering angle of π, or backscattering). For other relations of **S** to the radar scattering properties, see *Aydın* [2000].

Like with other scattering problems, the computational modeling of radar scattering from hydrometeors can be divided into two major components: a computational scattering algorithm that outputs the scattering properties given the properties of the radiation and a target that adheres to the requirements of the method, and a particle model that represents the target particle in the form expected by the scattering method. The computational scattering methods are summarized below in the context of hydrometeor radar scattering, while shape models are discussed in more detail in chapter 5.

2.1 Computational scattering methods

A large number of methods, different in their complexity and range of applicability, exist for computing electromagnetic scattering. Most computational electromagnetic scattering methods are based on solving the vector Helmholtz equation for the electric field **E** and the wavenumber k,

$$\nabla^2 \mathbf{E} + k^2 \mathbf{E} = 0, \tag{2.5}$$

with respect to the boundary conditions imposed at the boundaries of the scatterer. This equation uses the time harmonic properties of the electromagnetic field in waves to convert a time-dependent problem into a time-independent one. A notable exception to this among computational scattering methods is the finite difference time domain (FTDT) method, which involves a direct time-domain solution of Maxwell's equations.

Not all methods have been widely adopted for hydrometeors; below, an overview of the most common methods used to compute hydrometeor scattering is given. For a more thorough overview of currently used numerical methods in electromagnetic scattering, see *Kahnert* [2003].

2.1.1 Rayleigh approximation

The earliest theoretical explanation of scattering from particles was given, only a decade after the publication of Maxwell's equations, by *Lord Rayleigh* [1871] for particles that are much smaller than the incident wavelength. Rayleigh's scattering law, written in terms of the amplitude scattering matrix, gives

$$\mathbf{S} = \begin{bmatrix} S_1 & 0 \\ 0 & S_1 \cos(\theta) \end{bmatrix} \tag{2.6}$$

where θ is the scattering angle (*i.e.* the angle between the scattered and incident radiation),

$$S_1 = \frac{3k^2}{4\pi} KV \tag{2.7}$$

where V is the volume of the sphere, k is the wavenumber, and the dielectric factor $K = (n^2 - 1)/(n^2 + 2)$ and n is the complex refractive index.

The small-size assumption of the Rayleigh approximation is valid for most measurements by ground-based weather radars, which usually operate at wavelengths of roughly 5 cm (C band) or 11 cm (S band). This motivates the definition of radar reflectivity (see section 4.1.1), as the Rayleigh law dictates that the definitions of (4.1) and (4.2) are equivalent. With smaller wavelengths, practical situations where the Rayleigh approximation no longer holds are increasingly often encountered.

2.1.2 Mie theory

In order to estimate scattering in situations where Rayleigh's assumption no longer holds, *Mie* [1908] formulated an asymptotically exact convergent-series solution to the problem of scattering by spheres. In Mie's treatment, the incident and scattered waves and the internal field of the particle are expressed in terms of spherical wave functions. The full derivation of the Mie theory

is too extensive to detail here. For modern treatments of Mie theory, the reader is directed to *van de Hulst* [1957] or *Bohren and Huffman* [1983].

The Mie theory is strictly applicable only to spherical scatterers, but given the near-sphericity of raindrops, Mie theory has been commonly used to compute their scattering properties. As long as the size parameter of the particles is not too large and their refractive index not too high — and this is usually the case with hydrometeors — the Mie solution is quick to compute with a small computer program. Mie scattering programs are numerous and available for all commonly used platforms for scientific computing.

Mie theory can be generalized to spheres consisting of several layers, each with different optical properties [*Aden and Kerker*, 1951]. This allows the sphere model to approximate inhomogeneities in the structure of the scatterer.

2.1.3   *T*-matrix method

Waterman [1965] developed a generalized scattering formulation for non-spherical particles. As with Mie scattering, the electromagnetic fields are expanded in terms of basis functions. The *T* matrix relates the incident, internal and scattered field coefficient vectors $\mathbf{a}_{inc}$, $\mathbf{b}_{inc}$, $\mathbf{c}_{int}$, $\mathbf{d}_{int}$, $\mathbf{p}_{sca}$ and $\mathbf{q}_{sca}$ as

$$\begin{bmatrix} \mathbf{a}_{inc} \\ \mathbf{b}_{inc} \end{bmatrix} = \mathbf{Q} \begin{bmatrix} \mathbf{c}_{int} \\ \mathbf{d}_{int} \end{bmatrix} \tag{2.8}$$

$$\begin{bmatrix} \mathbf{p}_{sca} \\ \mathbf{q}_{sca} \end{bmatrix} = -\mathrm{Rg}\,\mathbf{Q} \begin{bmatrix} \mathbf{c}_{int} \\ \mathbf{d}_{int} \end{bmatrix} \tag{2.9}$$

from which it can be seen that the coefficients of the incident and scattered field expansions can be related by a matrix

$$\mathbf{T} = -\mathrm{Rg}\,\mathbf{Q}\,\mathbf{Q}^{-1}. \tag{2.10}$$

The matrices $\mathbf{Q}$ and $\mathrm{Rg}\,\mathbf{Q}$ are determined from surface integrals that depend on the shape of the particle.

The *T*-matrix method is technically not a computational scattering method by itself, but rather a formalism that can be used together with a number of methods for computing the *T* matrix, such as the null-field method (also known as the extended boundary condition method, EBCM) or the generalized point matching method [*Kahnert*, 2003]. Nevertheless, programs that use this formalism for numerical scattering computations are typically called *T*-matrix codes, and in applications (such as the papers presented in this thesis), it is common to refer to the scattering computations simply as *T*-matrix computations.

Regardless of the actual method used to compute the *T* matrix, it only needs to be calculated once for a given particle size and shape, and can then be used for any orientation or scattering geometry. This is a distinctive advantage of the formalism, as it means that for orientation averaging, commonly used in many applications including scattering by hydrometeors, the computationally intensive integrations and matrix inversions only need to be calculated once, and the scattering properties for the different orientations can be computed relatively quickly using analytical expressions.
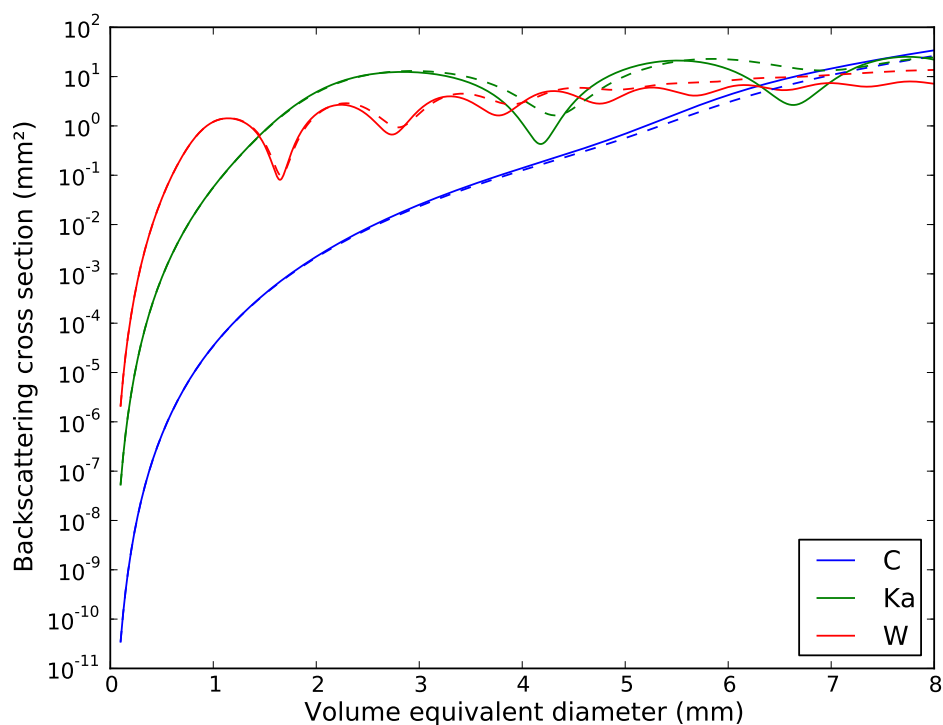
Figure 2.1: Backscattering cross sections of raindrops at horizontal polarization and horizontal incidence at C band (5.6 GHz; blue lines), K_a band (35.6 GHz; green lines) and W band (94.0 GHz; red lines). The solid lines correspond to raindrops with a fixed orientation (the symmetry axis oriented vertically), while the dashed lines were computed with orientation averaging with a 40° standard deviation in the canting angle from the vertical.

The *T*-matrix method can generally be used for a wide variety of shapes for which the surface of the particle is well defined: for example, *Laitinen and Lumme* [1998] presented a computer code that can compute the scattering properties of any star-shaped (convex with respect to a single interior point) particle. It can also be generalized to more than one scatterer [e.g. *Peterson and Ström*, 1973]; this is usually known as the cluster or superposition *T*-matrix method. However, the method is most commonly, especially for hydrometeors, applied on spheroids (spheres scaled along one axis). Spheroids are also quite accurate models of raindrops; *Thurai et al.* [2007] compared scattering results for spheroidal raindrops to those obtained for more accurate shapes and found that the differences were negligible except for the strengths and exact positions of the resonances.

Possibly the most widely used *T*-matrix code is that by *Mishchenko and Travis* [1998], which can perform the computations for spheroidal, cylindrical and Chebyshev particles. This code was used to produce the *T*-matrix results in Papers I–IV, with an interface to the Python programming language [*Leinonen*, 2013] enabling its direct integration to data analysis tools.

2.1.4   Discrete dipole approximation

In the Mie and *T*-matrix formulations, the particles are defined in terms of their surfaces. In contrast to this, *volume integral* methods convert the Helmholtz equation for the particle into a volume integral equation involving the incident and internal fields. The equation is of the form

$$\mathbf{E}(\mathbf{r}) = \mathbf{E}_{\mathrm{inc}}(\mathbf{r}) + \int_V (\varepsilon_r(\mathbf{r}') - 1)\mathbf{G}_0(\mathbf{r} - \mathbf{r}')\mathbf{E}(\mathbf{r})\, d\mathbf{r}' \tag{2.11}$$

where the integral is taken over the particle volume *V*. The dielectric constant $\varepsilon_r = n^2$ and the Green's tensor $\mathbf{G}_0$ is defined as

$$\mathbf{G}_0(\mathbf{r}) = \left(\mathbf{I} + \frac{1}{k^2}\nabla\nabla \right) \frac{\exp(ik|\mathbf{r}|)}{4\pi|\mathbf{r}|} \tag{2.12}$$

$$= \left(\mathbf{I} - \hat{\mathbf{e}}_r \otimes \hat{\mathbf{e}}_r + \left(\frac{i}{k|\mathbf{r}|} \right) \left(1 + \frac{i}{k|\mathbf{r}|} \right) \right.$$

$$\left. \left(\mathbf{I} - 3\hat{\mathbf{e}}_r \otimes \hat{\mathbf{e}}_r \right) \right) \frac{\exp(ik|\mathbf{r}|)}{4\pi|\mathbf{r}|} \tag{2.13}$$

where $\hat{\mathbf{e}}_r$ is the unit vector in the direction of **r** [*Lakhtakia and Mulholland*, 1993]. The integral equation is solved for the total internal field $\mathbf{E}(\mathbf{r})$, from which the scattering quantities are computed. The singularity of (2.13) at $\mathbf{r} = 0$ necessitates rigorous treatment of the integral of (2.11) in the immediate vicinity of that point; this gives rise to a "self-integral" whose treatment is summarized by *Kahnert* [2003].

Volume integral methods utilize a true three-dimensional, volumetric description of the particle. The direct consequence of this is that these methods can be used for arbitrary shapes and internal structures, limited only by the computational resources. On the other hand, it means that such a description is required even if the target could be modeled with a simpler shape that is accessible to faster methods, and thus the application of volume integral approach on such targets is typically wasteful.

The discrete dipole approximation (DDA; also known as the coupled dipole method, CDM) is an efficient and conceptually simple approximate solution of the volume integral equation. In it, the particle volume is subdivided into small regions in which the total electric field is assumed to be constant. This discretization is the approximation that is made in the DDA; otherwise the method is exact. The DDA can also be formulated by assuming that the scatterer consists of a finite number of discrete dipoles (hence the name) and that the polarizabilities of the dipoles give rise to electromagnetic interactions. These descriptions are now understood to be equivalent and are typically considered as a single method [*Lakhtakia and Mulholland*, 1993]. The former description is, in fact, a zeroth-order special case of the method of moments in electromagnetics, in which the field in each subregion is represented by basis functions.

With the discretization, (2.11) can written for *N* subregions as

$$\mathbf{E}(\mathbf{r}_i) \approx \mathbf{E}_{\mathrm{inc}}(\mathbf{r}_i) + \sum_{j=1}^{N} (\varepsilon_r(\mathbf{r}_j') - 1)\mathbf{G}_0(\mathbf{r}_i - \mathbf{r}_j)\mathbf{E}(\mathbf{r}_j). \tag{2.14}$$

All *N* vector equations can be expressed as a single system of $3N$ linear equations, which can be solved using standard techniques of linear algebra. The singularity of $\mathbf{G}_0$ when $i = j$ requires special treatments of those sum terms. Although the DDA was originally formulated by *Purcell and Pennypacker* [1973] using the Clausius-Mossotti polarizability for the "self term", the reasoning for using this simple form has been found theoretically unjustified, and various alternatives have been proposed, including the now-commonly used lattice dispersion relation (LDR) and filtered coupled dipoles (FCD). Different forms of the self term were compared by *Yurkin and Hoekstra* [2007].

The DDA generally requires that the size of the dipoles be small enough compared to the refractive index *n*, usually $|n|kd < 1.0$ or $|n|kd < 0.5$, where *d* is the diameter of the dipoles [*Zubko et al.*, 2010]. Beyond that, the DDA does not impose further restrictions on the positions or mutual sizes of the dipoles. However, *Goodman et al.* [1991] showed that the matrix-vector multiplication in the DDA system of equations can be written in terms of a three-dimensional discrete convolution and thus computed rapidly using the Fast Fourier Transform (FFT). This is a major advantage of the DDA in computational speed, compared to those integral equation methods that cannot utilize the FFT. The FFT technique is usually coupled with an iterative solver for the linear equations, such as the conjugate gradient method or one of its numerous variants. These improvements together enable the use of the DDA on problems that would otherwise be completely unrealistic. Indeed, a naive solution using Gaussian elimination combined with the above mentioned limits on the dipole size scales as $O(x^9)$ with scatterer size parameter *x*, rapidly overwhelming any available computing resources as the size increases. The combination of the FFT and an iterative solver reduces this to $O(x^{3+3\alpha} \log x)$, where N^α is the number of iterations required for the iterative method to converge.

One drawback of the FFT technique is that since it requires a regular grid, the empty dipoles in the problem domain must also be included in the data structure of the DDA implementation. This can be wasteful if the scatterer is very sparse. In these cases, a non-FFT solution may be preferable, especially if the memory requirements of the FFT solution are prohibitive.

Several computer implementations of the discrete dipole approximation exist, but two are in particularly widespread use: ADDA [*Yurkin and Hoekstra*, 2011] and DDSCAT [*Draine and Flatau*, 2012]. Both are free software and currently actively developed. ADDA was used in Papers II and IV–VI, with large targets in Paper VI computed using a non-FFT modification.

Scattering by raindrops is adequately modeled by the *T*-matrix method, and thus use of the more computationally intensive DDA is unnecessary. On the other hand, snowflakes and ice crystals are complex objects and as such present natural applications for the DDA, and have been modeled using it in several recent studies [*Liu*, 2004; *Kim*, 2006; *Petty and Huang*, 2010; *Adams and Bettenhausen*, 2012]. *Liu* [2008] has also established a database of scattering properties of ice crystals computed using the DDA. Other scattering methods that can be applied on nearly arbitrary shapes, functionally different but similar in capabilities to the DDA, have also been used to model snowflakes: *Ishimoto* [2008] used the finite difference time domain (FTDT) method, while *Botta et al.* [2010, 2011] used the generalized multiparticle Mie (GMM) method.

2.1.5   Rayleigh–Gans approximation

If the internal electromagnetic interactions of a scatterer are weak, they can be neglected, resulting in great simplification of the scattering computations. This is the idea of the Rayleigh–Gans approximation (RGA). It modifies (2.7) by introducing a form factor f:

$$S_1 = \frac{3k^2}{4\pi} K V f. \tag{2.15}$$

The form factor is defined as an integral of the phase of the electromagnetic wave over the particle volume V [*Bohren and Huffman*, 1983],

$$f = \frac{1}{V} \int_V \exp(i\delta(\mathbf{r})) \, d\mathbf{r} \tag{2.16}$$

$$\delta(\mathbf{r}) = k\mathbf{r} \cdot (\hat{\mathbf{e}}_z - \hat{\mathbf{e}}_s) \tag{2.17}$$

where the incident beam is assumed to be directed along the z-axis and $\hat{\mathbf{e}}_z$ is the unit vector along that axis; $\hat{\mathbf{e}}_s$ is a unit vector in the scattering direction. Thus, f accounts for the superposition of independently scattered waves from all parts of the particle. The generally accepted limits for the applicability of RGA are

$$|n - 1| \ll 1 \tag{2.18}$$

$$kD|n - 1| \ll 1, \tag{2.19}$$

but in the case of particles with a complex structure, it is not immediately clear what value should be used for the refractive index n (see also section 2.2). In Paper V, RGA was shown to be a good approximation for snowflakes in spite of the apparent failure of (2.18); this is because the sparse structure of snowflakes causes the effective refractive index to be much lower than that of bulk ice.

The Rayleigh–Gans approximation is very robust and applicable to many different formulations of the particle shape model, as (2.16) requires only that the function $\exp(i\delta(\mathbf{r}))$ be integrable over the particle domain. An interesting mathematical property that arises is the close mathematical connection of RGA to Fourier transforms. It is straightforward to show that the form factor is given by the Fourier transform of the particle mass distribution along an axis that is determined by the scattering direction. *Sorensen* [2001] treated this feature in much detail in the context of scattering from aggregate particles; it was also heavily exploited when building the theory in Paper VI.

2.2   Effective media

It is often necessary for the medium contained within the model particle to be homogeneous, as many methods in computational electromagnetic scattering require this. The mixture of different materials (ice and air for snowflakes; ice, water and air for melting snowflakes) in the real particle must then therefore be represented by a single effective medium, whose electromagnetic properties should be consistent with the real particle. Various suggestions regarding how this

effective-medium approximation (EMA) should be calculated have been given in the literature [e.g. *Bohren and Battan*, 1980; *Sihvola and Kong*, 1988; *Chýlek et al.*, 2000].

The most commonly used EMA is that of *Maxwell Garnett* [1904]. It assumes that two materials are mixed such that one component is present as small inclusions in the other component, called the matrix. For dielectric constants $\varepsilon_i = n_i^2$ and $\varepsilon_m = n_m^2$, and volume fractions of the inclusions f_i, the Maxwell-Garnett effective dielectric constant ε_{eff} is given by

$$f_i \frac{\varepsilon_i - \varepsilon_m}{\varepsilon_i + 2\varepsilon_m} = \frac{\varepsilon_{eff} - \varepsilon_m}{\varepsilon_{eff} + 2\varepsilon_m}. \tag{2.20}$$

The Maxwell-Garnett EMA is not symmetric with respect to the selection of the inclusion and the matrix, meaning that the result depends on how they are chosen, and it is often unclear how the selection should be made. The EMA of *Bruggeman* [1935] is symmetric with respect to the choice of materials 1 and 2, and is given by

$$f_1 \frac{\varepsilon_1 - \varepsilon_{eff}}{\varepsilon_1 + 2\varepsilon_{eff}} + f_2 \frac{\varepsilon_2 - \varepsilon_{eff}}{\varepsilon_2 + 2\varepsilon_{eff}} = 0. \tag{2.21}$$

Unfortunately, there is no obvious reason to select this over the Maxwell-Garnett EMA either, and there are more EMAs besides these, so it is often unclear which EMA one should use in a given case. However, if one component constitutes the clear minority of the mixture, it should satisfy the assumptions of the Maxwell-Garnett EMA if the minority component is treated as the inclusions and the majority component as the matrix. In that case, it should be justified to use that EMA.

3   Microphysics of precipitation

The formation of precipitation involves the evolution and interaction of individual hydrometeors. The larger-scale features of precipitation, which are usually of more interest in meteorological, hydrological or remote sensing applications, arise from these small-scale processes. The study of the microphysics of precipitation is concerned with the physical and statistical features of these processes. The overview given below is focused on the applications of precipitation microphysics that are related to remote sensing, and radars in particular.

3.1   Particle size distribution

A remote sensing system observes a large number of hydrometeors simultaneously. As the properties of individual particles are impossible to distinguish in the measured quantities, their properties must be considered statistically. The *particle size distribution* (PSD) $N(D)$ is a function that describes the distribution of the sizes of precipitation particles in a given atmospheric volume. The PSD specifies the number of particles in a unit volume for a diameter interval $[D, D + dD]$; in the context of precipitation, it is usually expressed in units of $\mathrm{mm}^{-1}\,\mathrm{m}^{-3}$. When the particles are liquid, the PSD is usually called the drop size distribution (DSD). For nonspherical raindrops, the diameter D is usually considered to be that of a spherical drop with the same volume, called the equal-volume diameter.

Integration over a PSD gives the total number concentration of hydrometeors, N_t:

$$N_t = \int_0^{D_{\max}} N(D)\, dD.$$

(3.1)

For raindrops, it is usually more interesting to calculate the total water mass content in a unit volume,

$$W = \frac{\pi}{6}\rho_w \int_0^{D_{\max}} D^3 N(D)\, dD$$

(3.2)

(where ρ_w is the density of water). The precipitation rate is given by

$$R = \int_0^{D_{\max}} v(D) D^3 N(D)\, dD$$

(3.3)

(where $v(D)$ is the hydrometeor fall velocity as a function of diameter). Various measures that give a characteristic size can also be derived. Obtaining the average particle size is straightforward,

but in a precipitation context, it is more common to use the mass-weighted mean diameter

$$D_m = \int_0^{D_{\max}} D^4 N(D) \, dD \Big/ \int_0^{D_{\max}} D^3 N(D) \, dD \qquad (3.4)$$

or the median volume diameter D_0, defined with

$$\int_0^{D_0} D^3 N(D) \, dD = \frac{1}{2} \int_0^{D_{\max}} D^3 N(D) \, dD, \qquad (3.5)$$

where $D_{\max}$ is the maximum particle size [*Bringi and Chandrasekar*, 2001]. Various parameters also exist that describe the shape of the distribution; a generic one is the mass-weighted distribution width

$$\sigma_m = \left(\int_0^{D_{\max}} (D - D_m)^2 D^3 N(D) dD \Big/ \int_0^{D_{\max}} D^3 N(D) \, dD \right)^{1/2}. \qquad (3.6)$$

As seen above, useful information about the PSD can be gained using just a few parameters. With this motivation, the PSD is usually expressed in a parametrized mathematical form. The simplest commonly used form is the exponential distribution

$$N(D) = N_0 \exp\left(-\Lambda D\right) \qquad (3.7)$$

with a rate parameter Λ and a scaling constant N_0, first used for raindrops by *Marshall and Palmer* [1948]. Later, to describe also the shape of the PSD, *Ulbrich* [1983] explored a gamma distribution with a shape parameter μ:

$$N(D) = N_0 D^\mu \exp\left(-\Lambda D\right) \qquad (3.8)$$

which reduces to the exponential distribution when $\mu = 0$. The main shortcoming of this model is that varying μ causes the total water content W to change, which introduces dependence between the parameters and thus complicates retrievals. This was addressed by the introduction of the concept of PSD "normalization" by, for example, *Chandrasekar and Bringi* [1987] and *Illingworth and Blackman* [1999]; later *Testud et al.* [2001] and *Illingworth and Blackman* [2002] presented a form of the gamma distribution where the total water content is the same for all values of μ, other PSD parameters being equal:

$$N(D) = N_w f(\mu) \left(\frac{D}{D_0} \right)^\mu \exp\left(-(3.67 + \mu) \frac{D}{D_0} \right) \qquad (3.9)$$

$$f(\mu) = \frac{6}{3.67^4} \frac{(3.67 + \mu)^{\mu+4}}{\Gamma(\mu + 4)}, \qquad (3.10)$$

relating the PSD directly to D_0, μ and the intercept parameter N_w. Figure 3.1 shows how such distributions compare with ones derived from measurements.

As it shall be explained in section 3.2, cloud ice and snow do not have a straightforward relation of mass and size like raindrops do, and defining their size through their maximal dimension is problematic. *Delanoë et al.* [2005] formulated another normalized gamma distribution that can be more suitable for those particles.
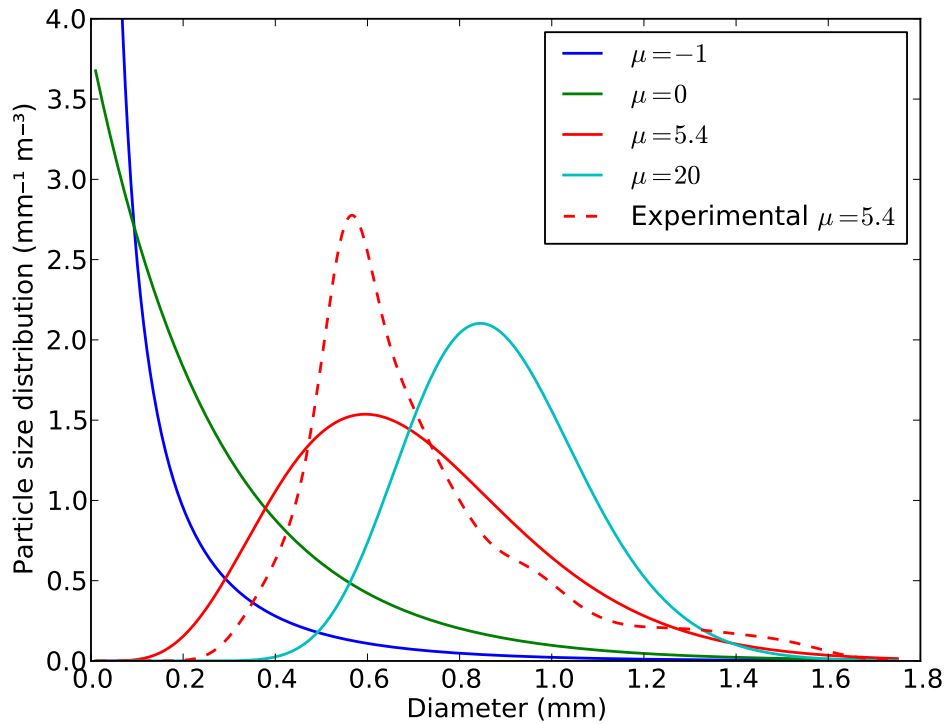
Figure 3.1: Example normalized gamma particle size distributions defined by (3.9) and (3.10) with $D_0 = 1$ mm and N_w set such that $\int N(D)\, dD = 1$ m^{-3}, with different values of the shape parameter μ. An experimental raindrop PSD from the dataset of Paper III with determined $D_0 \approx 1$ mm and $\mu \approx 5.4$ is shown for comparison.

Measured rain and snow size distributions have been noted to depend on the instrument integration time and on the sampling volume [*Jameson and Kostinski*, 2001]. Distributions tend to be more narrow and peaked for short time spans, but as the integration time is increased, the PSD tends to converge to the exponential form [*Kostinski and Jameson*, 1999]. Due to the spatial variability of the DSD, a time-integrated measurement at one point may not be representative of the corresponding radar measurement, which is almost instantaneous but encompasses a much larger volume. It is not clear how the integration time should be selected in order to achieve an *in situ* measurement that is comparable to radar measurements, or indeed if this is possible at all.

3.2 Evolution of hydrometeors

Micrometer-scale water droplets or ice crystals are nucleated in clouds. The droplets grow by condensation or deposition of more water vapor onto their surfaces. The details of the initial process are omitted here; see e.g. *Rogers and Yau* [1989] for more information. The formation of ice crystals requires either a sufficiently low temperature or suitable ice condensation nuclei; if the nuclei are scarce, water continues to stay in supercooled liquid form at temperatures down
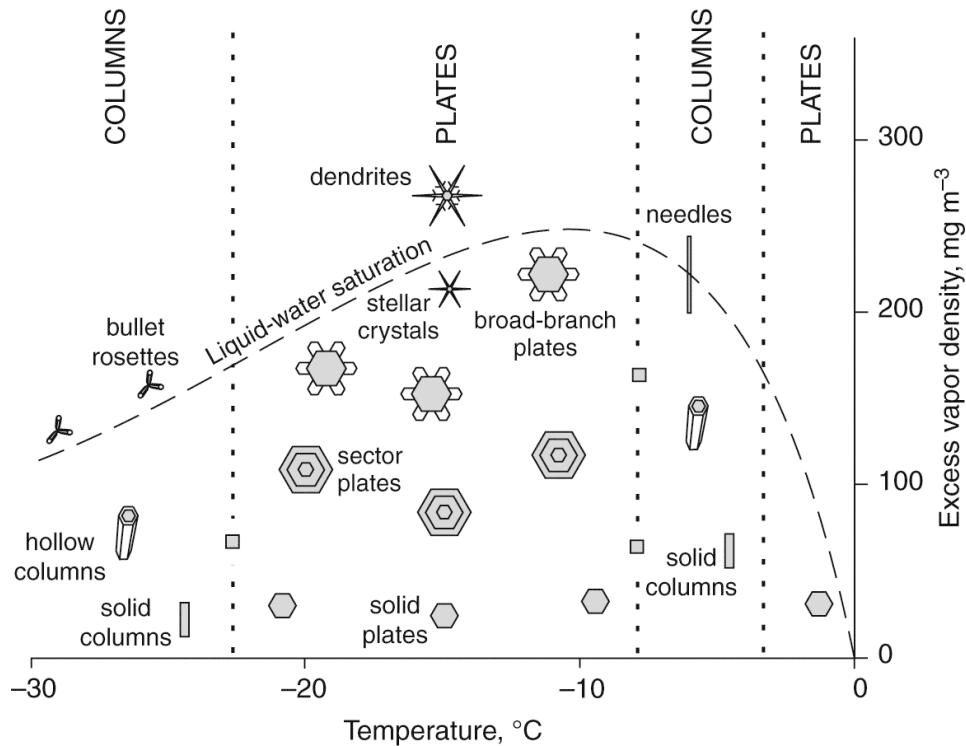
Figure 3.2: The types of snowflakes that form in different temperature and humidity conditions. From *Lamb and Verlinde* [2011], used with permission from Cambridge University Press.

to as low as $-30\,°C$ [*Hogan et al.*, 2003, 2004]. When ice crystals do nucleate, their properties are highly variable. The main factors determining the type of crystals that form are the ambient temperature and relative humidity; see Figure 3.2 for an overview of their effects. Depending on these factors, snowflakes may grow into "classical" branched snowflakes or different types, but also columns, plates, rosettes or needles. All of the shapes generally exhibit hexagonal symmetry, but imperfect crystals may grow in some conditions. The conditions may also vary during the growth process, leading to time-dependent growth patterns.

The cloud and precipitation particles grow further by colliding with each other. Colliding raindrops coalesce into new, larger drops. As raindrops grow, their fall velocity increases, enabling them to collect smaller, slower drops even more efficiently (the fall velocity can be calculated with the empirical formulas of *Atlas et al.* [1973] or *Thurai and Bringi* [2005]). As the size of the drops increases, their shape also changes from spherical to more oblate due to aerodynamic forcing [*Thurai and Bringi*, 2005]. The shape of a raindrop also oscillates due to aerodynamic forces; the effect of various oscillatory modes is commonly presented as variation in the *canting angle*, that is, the angle of the symmetry axis from the vertical. Drops that grow too big ($\gtrsim 8\,$mm) become unstable and tend to break up into several smaller drops. The collision-coalescence process is also not completely efficient and can create small secondary droplets.

A similar collision process causes snowflakes to grow, but the mechanisms for snowflake formation are, again, more varied [see, e.g., *Pruppacher and Klett*, 1997; *Lamb and Verlinde*, 2011].
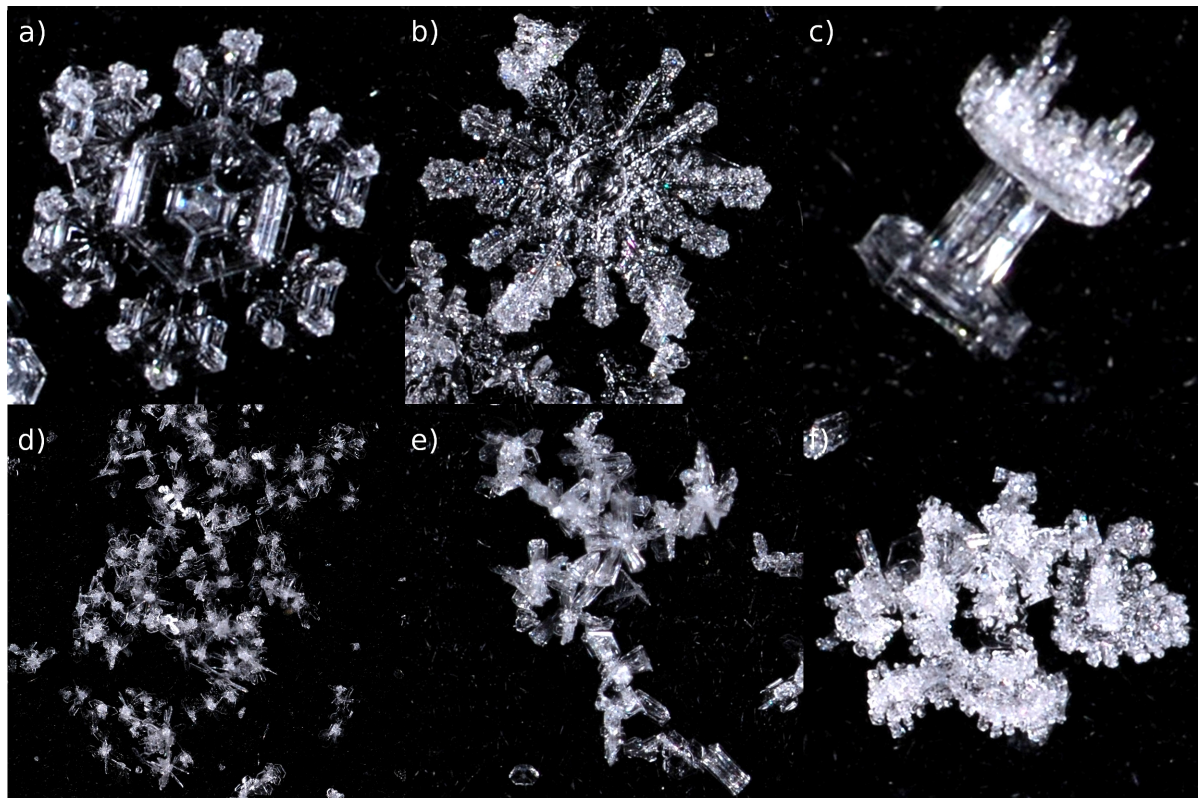
Figure 3.3: Different types of single-crystal, aggregate and rimed snowflakes (not in the same scale). a) A branched sector plate. b) An assemblage of two stellar crystals stacked on top of each other, resembling a 12-branch crystal. c) A rimed capped column. d) A large aggregate of sector plates. e) An aggregate of bullet rosettes. f) A rimed aggregate snowflake. The images are from the GPM Cold Season Precipitation Experiment [*Hudak et al.*, 2012], photo credits: Neil Fogg and Stephen Berg, University of Manitoba, used with permission.

Unlike raindrops, snowflakes are solid and thus do not coalesce on contact, but they may stick together — this is known as *aggregation*. Dendritic crystals, which grow at high water vapor supersaturations when the temperature is roughly between -12 and -17 °C, interlock mechanically due to their branched shapes, which makes them aggregate efficiently. Smoother ice crystals can stick together due to electrostatic forces or surface melting, but generally not as efficiently as dendrites. The relative importance of various sticking mechanisms is currently unclear. Snowflakes can also get rimed as they encounter varying amounts of supercooled cloud water droplets that freeze immediately on contact, forming small, spherical ice structures on the surface. Different types of single-crystal and aggregate snowflakes are shown in Figure 3.3.

It is generally recognized that snowflakes become less dense as they grow. For dendrite ice crystals, this is due to the fractal behavior of the branching associated with the growth of dendrites, while for aggregates, it is an inherent property of the process of aggregation (see section 2b of *Fabry and Szyrmer* [1999] for an explanation). The fractal growth gives rise to a

mass–dimensional (m–D) relation

$$m = \alpha D^{\beta} \tag{3.11}$$

where the scaling exponent is $0 < \beta \leq 3$ (the edge case $\beta = 3$ corresponding to "normal" growth such as that undergone by raindrops). Since the seminal study by *Magono and Nakamura* [1965], many *m–D* relations have been published. For aggregate snowflakes, β is usually of the order of 2, *Westbrook et al.* [2004] having provided a theoretical argument for $\beta = 2$. For denser snowflakes where riming is the dominant growth process, β is closer to 3. Although individual snowflakes may deviate significantly from the *m–D* relation, the snowflake ensemble is typically described using a single, average relation.

Once the hydrometeors grow large enough, they fall out of the clouds and continue the collision–aggregation process. At this stage, particles may also shrink through evaporation if they fall into subsaturated air.

4 Observation of precipitation

4.1 Radar observations

4.1.1 Radar reflectivity factor

Radars observe their targets remotely by transmitting a pulse of microwave radiation and receiving the echo. Weather radars relate the properties of the echo to the physical properties of the measured hydrometeors. In this section, the properties of weather radars that are important to the studies included in this thesis will be presented, with an emphasis on multi-frequency and polarimetric systems. For more general and comprehensive views of the topic, the reader is referred to the books by *Rinehart* [1991], *Doviak and Zrnić* [1993] and *Bringi and Chandrasekar* [2001].

The return signal of a weather radar depends on the number, size, shape and composition of the hydrometeors in the measurement volume. For small, spherical raindrops, the expected radar echo intensity is proportional to the sum of the sixth powers of the diameters of the drops in the measurement volume. This leads to the definition of the *(radar) reflectivity factor* as

$$Z = \sum_i D_i^6 = \int_0^{D_{\max}} N(D) D^6 \, dD, \tag{4.1}$$

where the summation is carried out over a unit volume, and i is the index of a particle in that volume. In the general case, the *equivalent reflectivity factor* is given by

$$Z_e = \frac{\lambda^4}{\pi^5 |K_w|^2} \int_0^{D_{\max}} \sigma(D) N(D) \, dD \tag{4.2}$$

where λ is the wavelength, the dielectric constant $K_w = (n_w^2 - 1)/(n_w^2 + 2)$ in which n_w is the complex refractive index of water, and $\sigma(D)$ is the average backscattering cross section of particles of diameter D. Z_e is defined such that for raindrops in the Rayleigh regime (drops much smaller than the radar wavelength), which applies for the majority of time with long-wavelength ground-based rain radars, the right-hand sides of (4.1) and (4.2) are equal, and thus $Z = Z_e$. At shorter wavelengths, commonly used in cloud radars and air- and space-based precipitation radars, the simple Rayleigh law and, consequently, the simple correspondence between Z and Z_e, breaks down. The reflectivity and equivalent reflectivity factors are also not equal for snowflakes due to the dielectric constant of snow being different from that of water.

The reflectivity factor is typically presented in logarithmic units of dBZ as $10 \log_{10}(Z_e/Z_0)$, where $Z_0 = 1 \, \text{mm}^{-6} \, \text{m}^{-3}$.

Equation (4.1) illustrates the general problem with radar measurements: the dependence of the reflectivity on the most interesting quantities — the water content W and the precipitation rate R — is not straightforward. Fortunately, the reflectivity still correlates with them in practice, and starting from *Marshall et al.* [1947], relations in the power-law form of

$$Z_e = aR^b \tag{4.3}$$

have been proposed by numerous authors in order to estimate R. For snow, empirical formulas that are climatologically correct on average, often called *Z–S* relations and usually of the same form as (4.3), can be formulated between the reflectivity and the snowfall rate in a similar fashion as with rain [*Sekhon and Srivastava*, 1970; *Smith*, 1984, among many].

The accuracy of the precipitation rate estimate is ultimately limited by the natural variation of the PSD. Quite different PSDs, and thus precipitation rates, can give the same radar reflectivity. The formulas like (4.3), used to estimate the precipitation rate from the reflectivity are empirical and correct on average at best, and the constants a and b depend on the climatic regime in which the measurements were made as well as the current weather conditions, in particular the distinction between stratiform and convective precipitation [*Austin*, 1987; *Atlas et al.*, 1999]. Even when used in the appropriate conditions, the random variability around this average relation is quite large. In snowfall rate estimation, the error is even higher than with rain because of the variability in the structure of snowflakes.

4.1.2 Errors in radar measurements

Radar measurements are subject to various error sources, which introduce both random and systematic errors. At a technological level, radars, like all electronic measurement systems, suffer from calibration uncertainty and receiver noise. Another source of random error originates from the statistical variation of the radar signal; this is usually mitigated by averaging over several pulses.

A systematic error, more difficult to predict than those mentioned before, is caused by the attenuation of radar pulses by the precipitation. The specific attenuation is usually measured in units of $dB\,km^{-1}$, and integrating it over a distance yields the path-integrated attenuation (PIA; in units of dB). As the intensity of precipitation can usually only be estimated from the reflectivity and other radar parameters, attenuation correction relies on these measurements. Thus, the correction is unstable because improper attenuation correction of the signal intensity can cause errors in the estimated reflectivity farther from the radar, which in turn further degrades the attenuation estimate, and so on. Attenuation can also be caused by the radome, especially when it is wet. Some of the signal lost through attenuation may be returned to the radar, albeit with incorrect range information, by multiple scattering from hydrometeors. Multiple scattering can be usually neglected as an error source, and is of most concern in W-band space-based radars [*Matrosov and Battaglia*, 2009], but it can sometimes also be found at K_u/K_a-bands and with airborne radars [*Battaglia et al.*, 2010a].

Additional errors (clutter) can be caused by echoes from the surface, buildings or vehicles being interpreted as meteorological, or by interference from external emitters at the frequency of the radar.

4.1.3   Dual-polarization methods

Dual-polarization radar measurements were suggested as a method to reduce the PSD-based uncertainty of rain rate retrievals already by *Seliga and Bringi* [1976], although they are only now gaining widespread adoption in operational use. Dual-polarization radars allow the measurement of many new quantities in addition to the reflectivity, but the most commonly used ones are the differential reflectivity, Z_{dr} and the specific differential phase, K_{dp}. Z_{dr} is simply the ratio $Z_{e,h}/Z_{e,v}$, where h and v refer to the horizontal and vertical polarizations, respectively, and is commonly given logarithmically in dB units. K_{dp} gives the rate of change in the relative signal phase of the two polarizations, usually expressed in $°\,\mathrm{km}^{-1}$. These are used either separately or together with the reflectivity to improve quantitative estimates of the rain rate. Formulas such as

$$R = a Z_{e,h}^{b} Z_{dr}^{c} \tag{4.4}$$

$$R = a K_{dp}^{b} \tag{4.5}$$

have been given by several authors; their use is summarized by *Bringi and Chandrasekar* [2001]. While still empirical in nature, these formulas constrain the rain rate more accurately than the simple *Z–R* relation. The K_{dp} based algorithms have been particularly popular in the estimation of heavy rain rates due to their lack of sensitivity to attenuation. *Ryzhkov et al.* [2005] proposed criteria to determine which estimation algorithm should be used, depending on the conditions.

The use of Z_{dr} and K_{dp} to improve rain rate retrievals is made possible by the fact that the oblateness of raindrops, which gives rise to the polarimetric quantities, depends directly on the size of the drops. Thus, a measurement of the oblateness yields information on the size, reducing uncertainty. In contrast, the information provided by polarimetry on falling snow is more uncertain because snow formation processes vary and thus the correspondence of size and shape is ambiguous and snowflake internal structure may have an effect on the polarimetric signature. That is not to say that polarimetric signals are not observed in snowfall; to the contrary, aligned snowflakes can give rise to high Z_{dr} and linear depolarization ratio (LDR) [*Vivekanandan et al.*, 1994; *Matrosov et al.*, 2005a; *Ryzhkov and Zrnic*, 2007]. However, the wide variety of different snowflakes found in nature makes it difficult to relate the polarimetric properties quantitatively to the physical ones.

4.1.4   Multi-frequency methods

The use of two or more beam-matched radars simultaneously at different wavelengths has been investigated as another method to estimate precipitation rate quantitatively. The retrieval methods allowed by dual-frequency radars can be divided roughly into two classes, attenuation-based and dual frequency ratio-based methods, although some algorithms combine both techniques. Early attempts at dual-frequency retrieval algorithms were mainly attenuation-based [e.g. *Eccles and Mueller*, 1971; *Goldhirsh and Katz*, 1974; *Eccles*, 1979], and derived the rain rate from the difference of the radar signal attenuation levels at two frequencies.

Many dual frequency ratio-based techniques have been suggested, especially for spaceborne radars, often following the approach of *Meneghini et al.* [1992]. These methods require at least one of the wavelengths to be in the Mie regime, on the order of the size of the measured hydrometeors, such that the equality $Z = Z_e$ no longer holds. Then, the ratio of the reflectivities at the two

frequencies (called the *dual-frequency ratio*, DFR) yields information about the size of the measured targets. This information can be used as a constraint that reduces the uncertainty of the PSD used in the the retrieval algorithm. The reflectivity is linearly proportional to the number density of hydrometeors in the target volume; as the DFR is a ratio, the number density is cancelled out and thus the DFR is not sensitive to it. This makes it an accurate estimator of the hydrometeor size: the only microphysical error source is the variation in the shape of the PSD, which is small compared to the variation in the number density.

Dual-wavelength radars have not been widely used operationally so far, and dual-polarization systems seem to offer a more cost-effective alternative for ground-based radar networks. However, dual-frequency retrieval algorithms do not require the direction of the radar beam to be near to horizontal, and thus dual-frequency radars have been adopted in many systems employing vertical or nearly vertical beams, such as many ground-based cloud radars as well as airborne and spaceborne cloud and precipitation radars. Dual-frequency radars that point at the surface, such as most airborne and spaceborne radars, can also extract information about the measured targets from the differential attenuation, or the difference in attenuation between the two signals. The differential attenuation can be determined if the difference of the surface echoes of the two frequencies is known, which is the case for ocean surfaces, but the great variation of the morphology of land surfaces makes this technique difficult to use over land.

Much of the development of dual-frequency radar algorithms has lately been motivated by their use in the GPM core satellite. Various versions and combinations of the above mentioned retrieval methods have been developed in connection to GPM [e.g. *Mardiana et al.*, 2004; *Liao and Meneghini*, 2005; *Rose and Chandrasekar*, 2005; *Nakamura and Iguchi*, 2007].

In contrast to polarimetric radars, the operational principle of dual-wavelength radars does not assume a correspondence between the shape and size of the targets. Thus, they also have been used as research tools for quantitative estimation of precipitation consisting of ice crystals, snowflakes and mixed-phase hydrometeors [*Matrosov*, 1993, 1998; *Matrosov et al.*, 2005b; *Liao et al.*, 2005].

4.1.5   Doppler radars

Another source of information about the precipitation target is the dependence of the radar return signal on the radial velocity of the targets relative to the radar. Weather radars that provide this information are called Doppler radars. With horizontally oriented radar beams, the Doppler velocity can be used to infer wind speeds. In vertical beam geometry, on the other hand, it can be used to infer vertical fall velocities. As these depend on hydrometeor type and size as well as vertical air motion, Doppler velocity can be used, together with other measurements, to retrieve these quantities.

4.2   *In situ* observations: disdrometers

As explained in section 4.1.1, radar measurements are sensitive to the size and shape of hydrometeors, in addition to the number of them. Rain gauges do not measure these quantities, and thus are unable to establish a complete "ground truth" that could be used as a reference for radar observation. To this end, and for lower-level study of precipitation microphysics, disdrometers have been

developed. These instruments observe individual hydrometeors and measure their size, and in some cases, their shape and velocity. With the measurement of a large number of drops, statistics about the size and shape can used to derive the particle size distribution. Below, some disdrometers that are closely related to the studies presented in this thesis, as well as particle imagers that can be used for the same purpose, are briefly introduced and compared. For a more thorough overview of the state of the art of disdrometers, see *Thurai and Bringi* [2008].

The *Joss-Waldvogel RD-69 disdrometer* (JWD or just RD-69) [*Joss and Waldvogel*, 1967] is one of the longest-used disdrometers. Still in active use in many places, this instrument measures electromechanically the impact force of raindrops that fall on its top metal plate. This force can be used to deduce the mass and, consequently, the diameter of the drops. In processing, the drop sizes are divided into 20 bins; the minimum measurable size is 0.32 mm. The JWD relies on the dependence of the fall velocity of a raindrop on its size, and thus will give erroneous results for the diameter when snow or hail is falling. Because the size–velocity relation is much more ambiguous for these types of hydrometeors, the JWD is unable to measure them correctly and they have to be filtered out manually if high data purity is desired. Up- and downdrafts can also temporarily influence the size–velocity relation, introducing errors.

The *Parsivel* optical disdrometer [*Löffler-Mang and Joss*, 2000] is nowadays in common use for hydrometeor size measurements. It uses a vertically thin, horizontally wide laser beam that is transmitted from one sensor head to another. Hydrometeors falling through the beam block it, and the width of the shadow can be measured at the receiver. The velocity of the particles is also measured, but this uses an assumption that the relationship between raindrop horizontal and vertical dimensions is uniquely determined by the size of the drop. For this reason, measuring the fall speed of other hydrometeors than raindrops is problematic [*Battaglia et al.*, 2010b].

A more sophisticated optical disdrometer than the Parsivel, the *Two-dimensional Video Disdrometer* (2DVD) [*Kruger and Krajewski*, 2002; *Randeu et al.*, 2002] uses two optical paths to measure hydrometeors. Both paths consist of a lamp, a Fresnel lens giving a uniform backlight, and a line scan camera measuring the shadow cast by hydrometeors falling through the measurement plane. The optical paths are vertically offset, and by matching particles detected at both planes and measuring the time difference, this instrument can determine their fall velocities and shapes without resorting to assumptions. This makes it more suitable for measuring the particle size distribution of snowflakes.

As an example of a different type of instrument that can be used this purpose, the *Particle Video Imager* (PVI), also known as the Snow Video Imager (SVI) [*Newman et al.*, 2009], is a video camera that captures pictures of backlit hydrometeors (typically snowflakes) within the focal area of the camera. Since it measures particles in a volume, not in a plane like the three disdrometers described above, the PVI measures the concentration of the particles in the air instead of the rainfall or snowfall rate at the ground. As a camera-based system, the PVI can also capture images of snowflakes and thus, it can be used to identify the types of snowflakes.

Some instruments measure raindrop size using microwave measurements instead. The Micro Rain Radar (MRR) is a small frequency-modulated continuous-wave radar that infers the raindrop sizes using Doppler fall velocity measurements and the drop size–velocity relation; for further information, see e.g. *Peters et al.* [2005]. The Precipitation Occurrence Sensor System (POSS) [*Sheppard*, 1990] is a similar system, but operates as a bistatic radar and with a much smaller

measurement volume.

The relative performance of the disdrometers has been studied in a number of papers. *Williams et al.* [2000] and *Tokay et al.* [2001] initially reported that the performance of 2DVD was slightly better than that of the JWD, and that the JWD was underestimating the number small drops significantly. However, *Tokay et al.* [2003] concluded that the underestimation was due to high acoustic noise levels around the JWD; in low-noise environments, the JWD may indeed be more sensitive to small drops than the 2DVD; similar results were found in Paper II of this thesis. *Tokay et al.* [2005] compared six collocated JWDs, and noted the importance of disdrometer comparisons for validating the measurements. In the Disdrometer Evaluation Experiment (DEVEX), *Krajewski et al.* [2006] found a reasonably good agreement between the 2DVD, Parsivel and another optical disdrometer called Dual Beam Spectropluviometer (DBS), 2DVD and DBS results being close to each other while differing somewhat more from the Parsivel results. *Thurai et al.* [2009] also compared the 2DVD axis ratios with wind tunnel measurements and found a close agreement, indicating that the mean axis ratios given by the 2DVD are reliable.

5 Snowflake models

5.1 Exact shape models

Snowflakes are complex targets, and so the generation of realistic snowflake models for use in scattering calculations is an important task. The different mechanisms of snowflake growth have to be taken into account to obtain realistic snowflakes.

In Paper II, one of the models used was the fractal-based snowflake generation algorithm of *Ishimoto* [2008]. This algorithm can create fluffy snowflakes with a user-defined fractal dimension, but as it uses only one fractal dimension, it does not accurately reproduce the change in the snowflake growth process with scale. In addition, it is only a phenomenological model of snowflake structure, and it is not clear which features of actual snowflakes it captures properly.

In Papers II and IV–VI, a physically based model of ice crystal aggregation was used to generate models of aggregate snowflakes. These were generated with computer codes based on that described by *Westbrook et al.* [2006]. These algorithms reproduce the physical process of aggregate formation more explicitly than the fractal algorithm. The exact aggregation algorithm was slightly different in each paper, as it was continuously developed further. Because of this, only the most advanced version, used in Paper VI, is described below in more detail.

First, the models of the individual crystals, called monomers, are created. Most of these are straightforward to define geometrically, but for dendritic crystals, a grid derived from the 2-dimensional hexagonal lattice-based algorithm by *Reiter* [2005] is used. From those prototypes, a given number of monomers of different sizes is created; their dimensions are determined with the empirical relations given by *Pruppacher and Klett* [1997]. The model monomers consist of small discrete volume elements that approximately cover the volume of the crystal. They are oriented according to a user-selected orientation distribution. These monomers are used as the initial set of particles.

The aggregation of the particles is modeled one step at a time. As snowflakes collide mainly due to their different fall velocities, the probability p_{ij} of two particles (indexed i and j) colliding is linearly proportional to the product of their mutual cross-sectional area and the difference in their terminal velocities. Neglecting constant factors and assuming that the aerodynamic drag force scales with the square of the velocity,

$$p_{ij} \propto (D_i + D_j)^2 \left| \sqrt{\frac{m_i}{D_i}} - \sqrt{\frac{m_j}{D_j}} \right| \tag{5.1}$$

where $m_{i,j}$ are the masses of the particles and $D_{i,j}$ are the diameters of their cross-sections in the direction of collision. On each step, two particles are selected for aggregation according to those
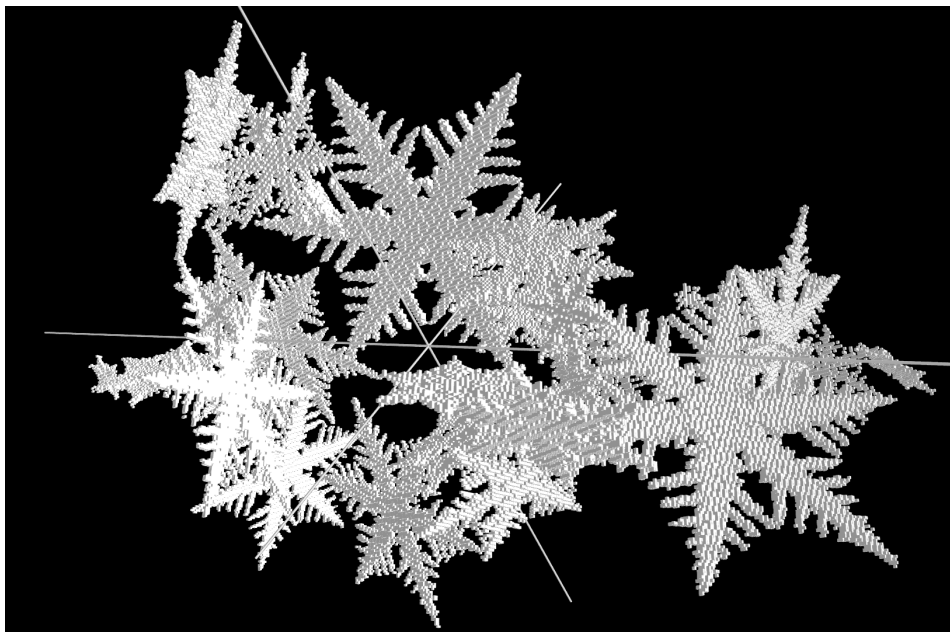
Figure 5.1: An example of a model aggregate, generated using the algorithm described in section 5.1. This aggregate consists of 35 dendrite crystals whose sizes have been sampled from the exponential distribution, and contains a total of 88 350 volume elements, each of which is 20 µm in diameter. The lines show the directions of the principal axes of the snowflake.

probabilities, and the point of contact is randomized. The particles are assumed to stick together rigidly at first contact; the realism of this assumption depends on the type of monomers, but aggregate snowflakes with very light mutual contact between the crystals are seen in nature. It can be a computationally intensive task to determine the exact point of collision at the volume element level; to accelerate the computation, the volume elements are spatially indexed using a quadtree structure that reduces the number of elements whose positions need to be compared. The newly-created aggregate is returned to the set of particles and new collision probabilities are computed; this process is continued until only one particle, containing all the originals, remains. The output of the aggregate generation algorithm is the combined set of volume elements of the now-connected crystals. The volume elements can be used directly as input for DDA codes. Figure 5.1 shows an example of an aggregate generated with this algorithm.

Aggregate particles can be generated with slightly different algorithms. Although some differences only affect the implementation, they can also often produce particles that, while visually similar, are somewhat different in their structure. For example, one method to generate aggregates, more straightforward than that given above, is to consider one particle as the aggregate and add crystal monomers one at a time. This, however, means that aggregates do not collide with each other in the process, which may cause subtle differences in the connectivity structure of the monomers. The process that was described above is intended to ensure that the model snowflakes exhibit realistic clustering.

5.2   Shape approximations

All computational snowflake models are, of course, approximations, as even the detailed volumetric models cannot reproduce the structural features whose scale is smaller than that of the volume units. However, the details at lengths much smaller than the wavelength are not very significant. As long as the distribution of mass is reproduced in a realistic way, those models can be called sufficiently accurate for practical purposes. Some physical processes such as breakup and riming are also not captured by the current version of the algorithm described in the previous section.

It is often desirable to approximate the shape of a complex particle also at larger scales. The reasons for this are twofold. Firstly, a simpler shape, typically a sphere or spheroid, is required by some computational methods such as Mie and *T*-matrix. Secondly, approximation of the shape reduces the number of free parameters in the particle model; in making the approximation, one hopes that it preserves the essential features of the particle in a much simpler description that is more accessible to inverse methods. It is worthwhile to point out the contrast between this type of structural simplification and that made in, for example, the Rayleigh–Gans approximation: a shape approximation simplifies the particle shape, and that "effective shape" is then usually used in a scattering method that is exact for those shapes, while the RGA simplifies the scattering model but not necessarily the shape model.

Many approximate shapes could be considered for snowflakes — a Gaussian mass distribution was found to be realistic in Paper VI — but homogeneous spheres or spheroids are by far the most common, and have been used as the basis of many conceptual models and retrieval schemes [e.g. *Bohren and Battan*, 1980; *Matrosov*, 2007; *Austin et al.*, 2009; *Hogan et al.*, 2012]. These models are usually constructed with density decreasing as the snowflakes become larger, as dictated by (3.11).

It is not obvious how the effective spheroid should be related to the properties of the particle. The model should conform to the Rayleigh approximation at the small-particle limit, and this (in addition to common sense) suggests that the masses of the exact and the approximate particle must be equal. While this presents its own practical difficulties because the mass of falling snowflakes is difficult to measure, it is a relatively straightforward requirement from the modeling point of view.

The size of the model particle is a more difficult parameter, as it can be defined in many ways, with no clear theoretical preference for any method. The largest physically justifiable shape approximation equates the maximum diameters of the spheroid and the snowflake; this is a practical solution as the maximum diameter is the easiest property to measure empirically. The smallest effective size that can be reasonably justified is given by the equal-volume principle: the ice in the particle is packed into a spheroid with no air inside. One approach that can capture some of the effect of the inhomogeneity of the exact particle is equating the radii of gyration R_g, defined as

$$R_g = \sqrt{\frac{1}{V} \int_V |\mathbf{r} - \mathbf{r}_{CM}|^2 \, d\mathbf{r}} \tag{5.2}$$

where $\mathbf{r}_{CM}$ is the center of mass. This usually leads to approximate particles whose size is somewhere between the above mentioned extremes. For other particles than snowflakes, other size relations have also been used, most notable the equal-surface-area method, but these are not vi-

able for snowflakes as the surface area is complicated to determine, and may even be ill defined for fractal shapes.

The aspect ratio of the effective spheroids is related to the lengths of the principal axes of the original particle. In practice, however, it is common to assume a fixed aspect ratio: 0.6 is supported by measurements for aggregates [*Korolev and Isaac*, 2003], while smaller aspect ratios may be used for single crystals.

6   Discussion

6.1   Summary of the results

The research presented in this thesis is focused on multi-frequency weather radars, their operational capabilities, and the interpretation and verification of their results. Special attention is given to considerations that are most relevant at the high latitudes: snowfall in Papers I, II and IV–VI and light rain in Paper III. Central to the treatment are the limits that the targets of observation, the hydrometeors, impose on the measurements of these radars.

Paper I of this thesis examines these limits with a method that can be used to simulate the snowfall observations of radars operating at different wavelengths from those that were used to make the measurement. Using data from those radars that were available for the measurements, one can thus estimate the capability of other types of radars, including those that currently in the design stage of development, to observe in that environment. Using an analysis of the microphysical variation of snowfall and validating the results with experimental data, it is shown that the equivalent radar reflectivity and specific attenuation of snow at one frequency can be estimated quite accurately if measurements are available at two other frequencies, one lower and the other higher than the desired frequency. Prediction using only one frequency is also possible, albeit with much greater margins of error.

Paper III also examines the limitations from a practical perspective: therein, the statistics of PSD parameters as well as radar reflectivity and other radar parameters from a five-year dataset are examined, and it is concluded that rain in the high latitudes is characterized by its light intensity and small drop size, which cause the precipitation there to be more difficult to measure remotely. Not only are radar sensitivity requirements higher in light rain, but small drops are usually in the Rayleigh scattering regime and also nearly spherical, reducing the usefulness of both dual-frequency and dual-polarization techniques. These notions are quantified by comparing the long-term statistics of radar parameters computed from the data to the sensitivities and measurement errors of existing ground-based and space-based radars.

Papers II and IV–VI, on the other hand, all focus on the observation of falling snow with radar. Paper II compares the results of DDA scattering calculations of two structurally detailed snowflake models, explained in section 5.1, to those obtained from the spheroidal shape model of snowflakes. This paper confirms that there are limits to the applicability of spheroid models of snowflakes for the purpose of interpreting radar observations. Although for small snowflakes (as compared to the radar wavelength), the spheroid and detailed models give equivalent results, and thus the spheroid model is valid, the discrepancy between them can be as large as orders of magnitude for large snowflakes. This suggests that spheroid models are unsuitable for physically

36

based retrievals when the snowflakes are large.

Paper II leaves open the question: is the nonspheroidal behavior of large snowflakes a relevant limitation in realistic snowfall cases? This is addressed in Paper IV using experimental triple-frequency data from the Wakasa Bay airborne radar experiment, analyzed using the method developed earlier by *Kneifel et al.* [2011]. The method, when applied on properly quality controlled data, permits the separation of spheroid-like and aggregate-like scattering behavior of snowflakes using the mutual behavior of two dual-frequency ratios. It is shown that in experimental data, such values sometimes occur that cannot be explained with the spheroid model using any realistic parameters, but which can be explained using detailed aggregate snowflakes instead. This way, it is shown that spheroids are indeed sometimes, though not always, unable to explain measurements of snowflakes consistently.

In Paper V, the modeling of snowflakes is approached from a slightly different perspective: instead of studying the applicability of simplified shape models, as with in Papers II and IV, this study concerns a simplified scattering model, the RGA (see section 2.1.5). The paper shows that the RGA estimate of the scattering properties of snowflakes is reasonably accurate for radar purposes and, furthermore, that the errors in the RGA-derived scattering properties are reasonably predictable. Thus, the faster and more analytically tractable RGA could be often used instead of the DDA, which was used for the reference computations.

Building on the results of Papers II, IV and V in particular, Paper VI presents an explanation as to *why* the spheroid models seem to work at small size parameters and fail at large size parameters. Using the RGA as a starting point, this paper showed that spheroids, which can be considered as models of the "average particle," fail because they implicitly assume that small-scale inhomogeneities are averaged out, while they still do, in fact, have an effect on the average scattering properties. It was shown using a simplified analytical model of snowflake structure that the average-particle model arises as a small size parameter approximation of the mathematically correct averaging model, which is based on the snowflake density autocorrelation function. Thus, the applicability of the spheroid model is inherently limited to the size range where it is valid to assume that the small-scale details do not have an appreciable effect.

6.2 Snowflake models: the way forward

Papers II and IV-VI address the question: what can one learn about snowflakes using a given set of multi-frequency radar observations? The particle shape model that captures the essential physical features of the snowflake, and is thereafter used to compute the scattering properties for the forward model, is identified by these papers as a crucial component in the quantitative estimation of snowfall by radar. The influence of the snowflake shape model and their relative benefits were analyzed from a number of viewpoints in these papers. Although it was not clear *a priori* how the shapes of snowflakes should ideally be modeled (nor can the question be considered to be completely answered now), the following qualities can be, usually implicitly, considered desirable for such particle models:

1. *Physical justifiability*: the model parameters, although they are used to compute the scattering quantities, should correspond also to the physical properties (mass, size, etc.) of the actual particle in some meaningful and well-defined way.

2. *Consistency*: it should be possible to represent a given real particle with the same model parameters throughout the range of applicability of the model. For example, the physical model of a given snowflake should not have to be changed if the wavelength changes.
3. *Simplicity*: the free parameters in a model should be descriptive, and few enough to allow them to be inferred using the given method of measurement.

Different models satisfy these requirements to different degrees. Volumetric snowflake models used with the discrete dipole approximation (DDA), consisting of tens or hundreds of thousands of volume elements, can be physically justifiable and consistent over the (large) range of applicability of DDA, but their lack of simplicity is severe. In contrast, sphere and spheroid models are generally physical (although this is not always the case) as well as simple, but as it was shown in Papers II and IV, they are not consistent over the full range of microwave wavelengths, and this inconsistency can be significant in naturally occurring cases. The notion of the range of applicability associated with the concept of model consistency may appear meaningless or tautological, as one can argue that the consistency, in fact, *defines* the range of applicability. Nevertheless, the requirement of consistency should be explicit and conscious to avoid the application of a model in a context where it is inconsistent, and hence invalid. As demonstrated in Papers IV and VI, such application may lead to misinterpretation of experimental results.

The shape model of the particle can be contrasted with the scattering model that is used to compute the scattering properties. Most scattering models, like the DDA and Mie, are at least asymptotically exact for their respective shape models, but some, such as the Rayleigh–Gans approximation, can be used for detailed shape models, but instead simplify the physics modeled by the scattering computations at the cost of exactness. The shape and scattering models are mutually dependent in the sense that detailed shape models require a scattering model that can use them, such as the DDA, while on the other hand the use of the DDA for spherical targets is unnecessarily complicated when a simpler scattering model like Mie theory yields the answer faster. However, as computers get faster, and well-documented and easily usable scattering programs become more prevalent, the choice of a scattering model depends increasingly on what advantages it brings to the analysis of the method and the results. This adds to the importance of the greatest advantage of the Rayleigh–Gans approximation, its analytical form and connection to Fourier analysis, as discussed in section 2.1.5. These allow the application of a variety of well-know mathematical results derived in other fields, the most significant of these being the Wiener–Khinchin theorem [*Mitra*, 2002] that relates the autocorrelation and the power spectrum as a Fourier transform pair. This connects the density autocorrelation function of a particle to the backscattering cross section as a function of frequency. The result of Paper V, that the Rayleigh–Gans approximation works quite well for snowflakes in practice, thus enabled the development of an autocorrelation-based snowflake model in Paper VI.

The fidelity of the shape model to the real particle is also a matter of the type of measurement that the model is used to interpret. The effective number of free parameters in the model should not be higher than the number of measurements made; otherwise the retrieval will be underdetermined. Parametrized particle size distributions, mass–dimensional relationships and effective-medium approximations are all tools that can be used to reduce the number of free parameters at the cost of decreased accuracy. Insightful selection of the particle model, and the parameters that are used to define it, can thus be used to reduce the uncertainty of retrievals, down to some lower limit

where no more information can be obtained using the given number of free parameters. As Paper VI demonstrated, a Gaussian mass distribution and the resulting density autocorrelation function provide a natural way to describe the shape and structure of snowflakes for scattering purposes. Using the autocorrelation approach, more complex models that convey more information about the snowflakes can be constructed.

Snowflake models should, then, be tuned to the type of measurement and the amount of information that the measurement conveys about the particle — they should be "as simple as possible, but no simpler". For example, the autocorrelation-based description is successful at describing the average particle in an ensemble because of the second-order nature of the statistics of scattering (*i.e.* the dependence on $|S|^2$). Conversely, additional measurements allow the use of a more detailed particle model that contains more information.

The combined results of Papers I–VI support the use of precipitation radars with two or more frequencies, of which at least one is in the millimeter-wave range, as instruments that can significantly improve precipitation retrieval performance over conventional single-frequency radars. There are two significant advantages to using multi-frequency systems: accuracy and complementarity. When several frequencies are used simultaneously, they can be used together for hydrometeor classification, and through their capability to resolve particle size, for quantitative precipitation estimation with improved accuracy. Also, it may be the case that one of the frequencies is unusable: that either the precipitation is too light to be detected using some (usually the lower) frequencies, or that it is too heavy and causes attenuation that blocks the signal of the higher frequencies. In those cases, multi-frequency systems can revert to using fewer frequencies and still remain operational. Millimeter-wave systems, which can generally achieve a better sensitivity then lower frequency radars with the same amount of power, are especially useful in spaceborne radars, in which the distance (typically 400 km for low Earth orbit) and the constraints on the available power impose a lower limit the minimum detectable signal. Also, the beam direction from orbit to the atmosphere is almost vertical, which limits the use of dual-polarization systems that rely on the aerodynamically driven vertical alignment of hydrometeors. This leaves multi-frequency radars, combined with radiometers, lidars or other additional instruments, as the most viable approach to increasing the information content of space-based precipitation remote sensing.

The improvement relative to single-frequency systems is particularly significant in the high latitudes, where snowfall is common and rain usually light. In these conditions, studies like that of Paper III and the experience from CloudSat have shown that a W-band radar with a high sensitivity (minimal detectable signal of around -30 dBZ) can improve the precipitation detection rate dramatically, compared to that of lower-frequency spaceborne radars. A beam-matched K_u- or K_a-band radar (or ideally, both) complementing the W-band radar would enable dual-frequency retrievals and provide full profiles also in areas where the attenuation is prohibitively high.

7   Concluding remarks

The importance of remote sensing in precipitation observations is likely to increase as the monitoring of the changing Earth system requires measurements that are continuous, global and accurate. The first two of the above-mentioned requirements are a matter of scale and resources; while these are obviously necessary, it is the last requirement, accuracy, that sets the fundamental limitations of a given remote sensing technology. This thesis is concerned with such limits in the context of multi-frequency weather radar systems, and the consequences of those limits for the use of such systems in the observation of precipitation, especially snow and light rain typically found in the high latitudes. Thorough understanding of the processes that determine the radar return signals not only helps one make the most out of data obtained using current measurements; it also enables the scientific community to allocate resources properly to the development and deployment of technology that can avoid, reduce or circumvent those limits.

As with all experimental systems, the limitations in the accuracy of multi-frequency radar measurements can be naturally divided into two main categories: those originating from practical limitations of the measurement setup, and those imposed by the information (and lack thereof) delivered by the measurement process. The former group includes such practical constraints as the available power and the effects of attenuation, and specifically for multi-frequency systems, the number of frequencies that can be used simultaneously. One's capability to verify the accuracy of the measurements, a topic that Papers I and III pertain to, is another practical constraint.

Although the practical limits are considered in this thesis, it is the examination of the extent of possible measurements by multi-frequency systems that defines its primary substance. The interplay between these theoretical possibilities and the practical considerations ultimately determines the capabilities of a measurement system. For example, as demonstrated in Paper VI, the maximum amount of information obtainable by a multi-frequency radar about the average physical structure of measured snowflakes can be obtained with simultaneous measurements at all frequencies, and even this ideal situation, their exact physical structure cannot be determined. Furthermore, one usually only has at most a few beam-matched radars at different frequencies simultaneously available, and must thus resort to interpolation, extrapolation and assumptions to overcome these practical limitations.

The use of an appropriate snowflake model, which is used to define the structural properties of a particle in such a way that the scattering properties can be calculated, is important for the examination of snowfall measurements by multi-frequency radars. Simple models defined using the average particle shape are only applicable in specific circumstances. In many practical cases, knowledge about the small-scale structure of the hydrometeor is required to model the multi-frequency scattering accurately and consistently. This can be achieved by using detailed particle models that are created with an algorithm accounting for the physics of snowflake formation, and

by computing the scattering properties with a method that can work on arbitrarily shaped targets.

While highly detailed hydrometeor and scattering models may enable more accurate retrievals, the conceptual elegance of simple particle models should not be ignored. Spheroidal models of snowflakes are certainly perfectly valid in the Rayleigh regime and well beyond it (as evidenced by Papers IV and VI), and there appears to be no need to adopt anything more sophisticated at the K_u band or lower frequencies. The simplicity of a model also provides conceptual clarity that can allow one to distinguish the essential features of the scattering by a target. The formulation of Paper VI would not have been possible without the underlying elegance of the Rayleigh–Gans approximation. As for the validity of using spherical shape models, the following quote from *Bohren and Huffman* [1983] resonates particularly well with the results of this thesis:

> On the one hand, there are those who scoff at the use of Mie theory to describe any properties of nonspherical particles [...]; on the other hand, there are those who unquestioningly use Mie theory for any and every aspect of light interaction with such particles. Neither attitude is enlightened. The Mie theory, limited though it may be, does provide a first-order description of optical effects in nonspherical particles, and it correctly describes many small-particle effects that are not intuitively obvious.

One can, then, conclude that despite the limitations identified in this thesis and by many others, there is reason for optimism. Multi-frequency weather radar systems that employ millimeter-wave channels do appear to be the way forward, particularly for space-based precipitation remote sensing. They offer a flexible measurement setup whose principles have a robust foundation in theory. The GPM core satellite will be the pathfinder for the practical realizations of such systems in Earth orbit, and it is certainly the author's hope and recommendation that more follow in its footsteps.

References

Adams, I. S., and M. H. Bettenhausen (2012), The scattering properties of horizontally aligned snow crystals and crystal approximations at millimeter wavelengths, *Radio Sci.*, RS5007, doi:10.1029/2012RS005015.

Aden, A. L., and M. Kerker (1951), Scattering of electromagnetic waves from two concentric spheres, *J. Appl. Phys.*, *22*(10), 1242–1246, doi:10.1063/1.1699834.

Atlas, D., R. C. Srivastava, and R. S. Sekhon (1973), Doppler radar characteristics of precipitation at vertical incidence, *Rev. Geophys.*, *11*(1), 1–35, doi:10.1029/RG011i001p00001.

Atlas, D., C. W. Ulbrich, F. D. Marks Jr., E. Amitai, and C. R. Williams (1999), Systematic variation of drop size and radar-rainfall relations, *J. Geophys. Res.*, *104*(D6), 6155–6169.

Austin, P. M. (1987), Relation between measured radar reflectivity and surface rainfall, *Mon. Wea. Rev.*, *115*(5), 1053–1070, doi:10.1175/1520-0493(1987)115<1053:RBMRRA>2.0.CO;2.

Austin, R. T., A. J. Heymsfield, and G. L. Stephens (2009), Retrieval of ice cloud microphysical parameters using the CloudSat millimeter-wave radar and temperature, *J. Geophys. Res.*, *114*, D00A23, doi:10.1029/2008JD010049.

Aydın, K. (2000), Centimeter and millimeter wave scattering from hydrometeors, in *Light Scattering by Nonspherical Particles*, edited by M. I. Mishchenko, J. W. Hovenier, and L. D. Travis, chap. 16, Academic Press.

Battaglia, A., S. Tanelli, S. Kobayashi, D. Zrnic, R. J. Hogan, and C. Simmer (2010a), Multiple-scattering in radar systems: A review, *J. Quant. Spectrosc. Radiat. Transfer*, *111*(6), 917–947, doi:10.1016/j.jqsrt.2009.11.024.

Battaglia, A., E. Rustemeier, A. Tokay, U. Blahak, and C. Simmer (2010b), PARSIVEL snow observations: A critical assessment, *J. Atmos. Oceanic Technol.*, *27*, 333–344, doi:10.1175/2009JTECHA1332.1.

Bohren, C. F., and L. J. Battan (1980), Radar backscattering by inhomogeneous precipitation particles, *J. Atmos. Sci.*, *37*(8), 1821–1827, doi:10.1175/1520-0469(1980)037<1821:RBBIPP>2.0.CO;2.

Bohren, C. F., and D. R. Huffman (1983), *Absorption and Scattering of Light by Small Particles*, John Wiley & Sons, Inc.

Botta, G., K. Aydin, and J. Verlinde (2010), Modeling of microwave scattering from cloud ice crystal aggregates and melting aggregates: A new approach, *IEEE Geosci. Remote Sens. Lett.*, *7*(3), 572–576, doi:10.1109/LGRS.2010.2041633.

Botta, G., K. Aydin, J. Verlinde, A. E. Avramov, A. S. Ackerman, A. M. Fridlind, G. M. McFarquhar, and M. Wolde (2011), Millimeter wave scattering from ice crystals and their aggregates: Comparing cloud model simulations with X-and Ka-band radar measurements, *J. Geophys. Res.*, *116*, D00T04, doi:10.1029/2011JD015909.

Bringi, V. N., and V. Chandrasekar (2001), *Polarimetric Doppler weather radar: principles and applications*, Cambridge University Press.

Bruggeman, D. A. G. (1935), Berechnung verschiedener physikalischer Konstanten von heterogenen Substanzen. I. Dielektrizitätskonstanten und Leitfähigkeiten der Mischkörper aus isotropen Substanzen, *Annalen der Physik*, *416*(7), 636–664, doi:10.1002/andp.19354160705.

Chandrasekar, V., and V. N. Bringi (1987), Simulation of radar reflectivity and surface measurements of rainfall, *J. Atmos. Oceanic Technol.*, *4*(3), 464–478.

Chýlek, P., G. Videen, D. J. W. Geldart, J. S. Dobbie, and H. C. W. Tso (2000), Effective medium approximations for heterogeneous particles, in *Light Scattering by Nonspherical Particles*, edited by M. I. Mishchenko, J. W. Hovenier, and L. D. Travis, chap. 9, Academic Press.

Delanoë, J., A. Protat, J. Testud, D. Bouniol, A. Heymsfield, A. Bansemer, P. R. A. Brown, and R. M. Forbes (2005), Statistical properties of the normalized ice particle size distribution, *J. Geophys. Res.*, *110*, D10201, doi:10.1029/2004JD005405.

Doviak, R. J., and D. S. Zrnić (1993), *Doppler Radar and Weather Observations*, 2 ed., Academic Press.

Draine, B. T., and P. J. Flatau (2012), User guide for the discrete dipole approximation code DDSCAT 7.2, arXiv:1202.3424.

Eccles, P. (1979), Comparison of remote measurements by single- and dual-wavelength meteorological radars, *IEEE Trans. Geosci. Electron.*, *17*(4), 205–218, doi:10.1109/TGE.1979.294650.

Eccles, P. J., and E. A. Mueller (1971), X-band attenuation and liquid water content estimation by a dual-wavelength radar, *J. Appl. Meteor.*, *10*(6), 1252–1259, doi:10.1175/1520-0450(1971)010<1252:XBAALW>2.0.CO;2.

Ellis, T. D., T. L'Ecuyer, J. M. Haynes, and G. L. Stephens (2009), How often does it rain over the global oceans? the perspective from CloudSat, *Geophys. Res. Lett.*, *36*, L03815, doi:10.1029/2008GL036728.

Fabry, F., and W. Szyrmer (1999), Modeling of the melting layer. Part II: Electromagnetic, *J. Atmos. Sci.*, *56*, 3593–3600, doi:10.1175/1520-0469(1999)056<3593:MOTMLP>2.0.CO;2.

Goldhirsh, J., and I. Katz (1974), Estimation of raindrop size distribution using multiple wavelength radar systems, *Radio Sci.*, *9*(4), 439–446, doi:10.1029/RS009i004p00439.

Goodman, J. J., B. T. Draine, P. J. Flatau, et al. (1991), Application of fast-fourier-transform techniques to the discrete-dipole approximation, *Opt. Lett.*, *16*(15), 1198–1200, doi:10.1364/OL.16.001198.

Haynes, J. M., T. S. L'Ecuyer, G. L. Stephens, S. D. Miller, C. Mitrescu, N. B. Wood, and S. Tanelli (2009), Rainfall retrieval over the ocean with spaceborne W-band radar, *J. Geophys. Res.*, *114*, D00A22, doi:10.1029/2008JD009973.

Heino, R., and E. Hellsten (1983), Climatological Statistics in Finland, in *Meteorological Yearbook of Finland*, vol. 80, Finnish Meteorological Institute.

Hogan, R. J., A. J. Illingworth, E. J. O'Connor, and J. P. V. Poiares Baptista (2003), Characteristics of mixed-phase clouds. ii: A climatology from ground-based lidar, *QJRMS*, *129*(592), 2117–2134, doi:10.1256/qj.01.209.

Hogan, R. J., M. D. Behera, E. J. O'Connor, and A. J. Illingworth (2004), Estimate of the global distribution of stratiform supercooled liquid water clouds using the LITE lidar, *Geophys. Res. Lett.*, *31*(5), L05,106, doi:10.1029/2003GL018977.

Hogan, R. J., L. Tian, P. R. A. Brown, C. D. Westbrook, A. J. Heymsfield, and J. D. Eastment (2012), Radar backscattering by inhomogeneous precipitation particles, *J. Appl. Meteor. Climatol.*, *51*, 655–671, doi:10.1175/JAMC-D-11-074.1.

Hudak, D., W. Petersen, G. Skofronick-Jackson, M. Wolde, C. Derksen, K. Strawbridge, P. Kollias, and R. Stewart (2012), GPM cold season precipitation experiment (GCPEx), in *2012 EUMETSAT Meteorological Satellite Conference*.

Hélière, A., A. Lefebvre, T. Wehr, J.-L. Bézy, and Y. Durand (2007), The earthcare mission: Mission concept and lidar instrument pre-development, in *IEEE Geoscience and Remote Sensing Symposium, 2007*, pp. 4975–4978, doi:10.1109/IGARSS.2007.4423978.

Iguchi, T., R. Oki, E. A. Smith, and Y. Furuhama (2002), Global Precipitation Measurement program and the development of dual-frequency precipitation radar, *J. Commun. Res. Lab.*, *49*(2), 37–45.

Illingworth, A. (2004), Improved precipitation rates and data quality by using polarimetric measurements, in *Weather Radar: Principles and Advanced Applications*, edited by P. Meischner, chap. 5, pp. 130–166, Springer.

Illingworth, A. J., and T. M. Blackman (1999), The need to normalise RSDs based on the gamma RSD formulations and implications for interpreting polarimetric radar data., in *29th International Conference on Radar Meteorology*.

Illingworth, A. J., and T. M. Blackman (2002), The need to represent raindrop size spectra as normalized gamma distributions for the interpretation of polarization radar observations, *J. Appl. Meteor.*, *41*(3), 286–297, doi:10.1175/1520-0450(2002)041<0286:TNTRRS>2.0.CO;2.

Ishimoto, H. (2008), Radar backscattering computations for fractal-shaped snowflakes, *J. Meteor. Soc. Japan*, *86*(3), 459–469, doi:10.2151/JMSJ.86.459.

Jameson, A. R., and A. B. Kostinski (2001), What is a raindrop size distribution?, *Bull. Amer. Meteor. Soc.*, *82*, 1169–1177, doi:10.1175/1520-0477(2001)082<1169:WIARSD>2.3.CO;2.

Joe, P., et al. (2010), The polar precipitation measurement mission, in *European Conference on Radar in Meteorology and Hydrology, 2010*.

Joss, J., and A. Waldvogel (1967), A raindrop spectrograph with automatic analysis, *Pure Appl. Geophys.*, *68*, 240–246.

Kahnert, F. M. (2003), Numerical methods in electromagnetic scattering theory, *J. Quant. Spectrosc. Radiat. Transfer*, *79*, 775–824, doi:10.1016/S0022-4073(02)00321-7.

Kim, M. J. (2006), Single scattering parameters of randomly oriented snow particles at microwave frequencies, *J. Geophys. Res.*, *111*, D14201, doi:10.1029/2005JD006892.

Kneifel, S., M. S. Kulie, and R. Bennartz (2011), A triple frequency approach to retrieve microphysical snowfall parameters, *J. Geophys. Res.*, *116*, D11203, doi:10.1029/2010JD015430.

Korolev, A., and G. Isaac (2003), Roundness and aspect ratio of particles in ice clouds, *J. Atmos. Sci.*, *60*(15), 1795–1808, doi:10.1175/1520-0469(2003)060<1795:RAAROP>2.0.CO;2.

Kostinski, A. B., and A. R. Jameson (1999), Fluctuation properties of precipitation. Part III: On the ubiquity and emergence of the exponential drop size spectra, *J. Atmos. Sci.*, *56*(1), 111–121, doi:10.1175/1520-0469(1999)056<0111:FPOPPI>2.0.CO;2.

Kozu, T., et al. (2001), Development of Precipitation Radar Onboard the Tropical Rainfall Measuring Mission (TRMM) Satellite, *IEEE Trans. Geosci. Remote Sens.*, *39*(1), 102–116.

Krajewski, W. F., et al. (2006), DEVEX-Disdrometer Evaluation Experiment: Basic results and implications for hydrologic studies, *Adv. Water Resour.*, *29*(2), 311–325, doi:10.1016/j.advwatres.2005.03.018.

Kruger, A., and W. F. Krajewski (2002), Two-dimensional video disdrometer: A description, *J. Atmos. Oceanic Technol.*, *19*, 602–617, doi:10.1175/1520-0426(2002)019<0602:TDVDAD>2.0.CO;2.

Kummerow, C., W. Barnes, T. Kozu, J. Shiue, and J. Simpson (1998), The Tropical Rainfall Measuring Mission (TRMM) sensor package, *J. Atmos. Oceanic Technol.*, *15*(3), 809–817, doi:10.1175/1520-0426(1998)015<0809:TTRMMT>2.0.CO;2.

Kummerow, C., et al. (2000), The status of the Tropical Rainfall Measuring Mission (TRMM) after two years in orbit, *J. Appl. Meteor.*, *39*(12), 1965–1982, doi:10.1175/1520-0450(2001)040<1965:TSOTTR>2.0.CO;2.

Laitinen, H., and K. Lumme (1998), *T*-matrix method for general star-shaped particles: First results, *J. Quant. Spectrosc. Radiat. Transfer*, *60*(3), 325–334, doi:10.1016/S0022-4073(98)00009-0.

Lakhtakia, A., and G. W. Mulholland (1993), On two numerical techniques for light scattering by dielectric agglomerated structures, *J. Res. Natl. Inst. Stand. Technol.*, *98*(6), 699–716.

Lamb, D., and J. Verlinde (2011), *Physics and Chemistry of Clouds*, Cambridge University Press.

Leinonen, J. (2013), Python code for T-matrix scattering calculations, available online at http://code.google.com/p/pytmatrix/.

Leinonen, J., D. Moisseev, V. Chandrasekar, and J. Koskinen (2011), Mapping radar reflectivity values of snowfall between frequency bands, *IEEE Trans. Geosci. Remote Sens.*, *49*(8), 3047–3058, doi:10.1109/TGRS.2011.2117432.

Leinonen, J., D. Moisseev, M. Leskinen, and W. Petersen (2012a), A climatology of disdrometer measurements of rainfall in Finland over five years with implications for global radar observations, *J. Appl. Meteor. Climatol.*, *51*, 392–404, doi:10.1175/JAMC-D-11-056.1.

Leinonen, J., S. Kneifel, D. Moisseev, J. Tyynelä, S. Tanelli, and T. Nousiainen (2012b), Nonspheroidal behavior in millimeter-wavelength radar observations of snowfall, *J. Geophys. Res.*, *117*, D18205, doi:10.1029/2012JD017680.

Leinonen, J., D. Moisseev, and T. Nousiainen (2013), Linking snowflake microstructure to multi-frequency radar observations, *J. Geophys. Res.*, *118*, doi:10.1002/jgrd.50163.

Lemke, P., et al. (2007), Observations: Changes in Snow, Ice and Frozen Ground, in *Climate Change 2007: The Physical Science Basis. Contribution of Working Group I to the Fourth Assessment Report of the Intergovernmental Panel on Climate Change*, chap. 4, pp. 337–383, Cambridge University Press.

Liao, L., and R. Meneghini (2005), A study of air/space-borne dual-wavelength radar for estimation of rain profiles, *Adv. in Atmos. Sci.*, *22*(6), 841–851, doi:10.1007/BF02918684.

Liao, L., R. Meneghini, T. Iguchi, and A. Detwiler (2005), Use of dual-wavelength radar for snow parameter estimates, *J. Atmos. Oceanic Technol.*, *22*(10), 1494–1506, doi:10.1175/JTECH1808.1.

Lim, S., V. Chandrasekar, and V. N. Bringi (2005), Hydrometeor classification system using dual-polarization radar measurements: Model improvements and in situ verification, *IEEE Trans. Geosci. Remote Sens.*, *43*(4), 792–801, doi:10.1109/TGRS.2004.843077.

Liu, G. (2004), Approximation of single scattering properties of ice and snow particles for high microwave frequencies, *J. Atmos. Sci.*, *61*(20), 2441–2456, doi:10.1175/1520-0469(2004)061<2441:AOSSPO>2.0.CO;2.

Liu, G. (2008), A database of microwave single-scattering properties for nonspherical ice particles, *Bull. Amer. Meteor. Soc.*, *89*(10), 1563–1570, doi:10.1175/2008BAMS2486.1.

Löffler-Mang, M., and J. Joss (2000), An optical disdrometer for measuring size and velocity of hydrometeors, *J. Atmos. Oceanic Technol.*, *17*(2), 130–139, doi:10.1175/1520-0426(2000)017<0130:AODFMS>2.0.CO;2.

Magono, C., and T. Nakamura (1965), Aerodynamic studies of falling snowflakes, *J. Meteor. Soc. Japan*, *43*(3), 139–147.

Mardiana, R., T. Iguchi, and N. Takahashi (2004), A dual-frequency rain profiling method without the use of a surface reference technique, *IEEE Trans. Geosci. Remote Sens.*, *42*(10), 2214–2225, doi:10.1109/TGRS.2004.834647.

Marshall, J. S., and W. M. Palmer (1948), The distribution of raindrops with size, *J. Meteor.*, *5*(4), 165–166, doi:10.1175/1520-0469(1948)005<0165:TDORWS>2.0.CO;2.

Marshall, J. S., R. C. Langille, and W. M. Palmer (1947), Measurement of rainfall by radar, *J. Meteor.*, *4*(6), 186–192, doi:10.1175/1520-0469(1947)004<0186:MORBR>2.0.CO;2.

Matrosov, S. Y. (1993), Possibilities of cirrus particle sizing from dual-frequency radar measurements, *J. Geophys. Res.*, *98*, 20,675–20,683, doi:10.1029/93JD02335.

Matrosov, S. Y. (1998), A dual-wavelength radar method to measure snowfall rate, *J. Appl. Meteor.*, *37*(11), 1510–1521, doi:10.1175/1520-0450(1998)037<1510:ADWRMT>2.0.CO;2.

Matrosov, S. Y. (2007), Modeling backscatter properties of snowfall at millimeter wavelengths, *J. Atmos. Sci.*, *64*, 1727–1736, doi:10.1175/JAS3904.1.

Matrosov, S. Y., and A. Battaglia (2009), Influence of multiple scattering on CloudSat measurements in snow: A model study, *Geophys. Res. Lett.*, *36*, L12806, doi:10.1029/2009GL038704.

Matrosov, S. Y., R. F. Reinking, and I. V. Djalalova (2005a), Inferring fall attitudes of pristine dendritic crystals from polarimetric radar data, *J. Atmos. Sci.*, *62*(1), 241–250, doi:10.1175/JAS-3356.1.

Matrosov, S. Y., A. J. Heymsfield, and Z. Wang (2005b), Dual-frequency radar ratio of nonspherical atmospheric hydrometeors, *Geophys. Res. Lett.*, *32*, L13816, doi:10.1029/2005GL023210.

Maxwell Garnett, J. C. (1904), Colours in metal glasses and in metallic films., *Phil. Trans. R. Soc. London A*, *203*, 385–420, doi:10.1098/rsta.1904.0024.

Meneghini, R., T. Kozu, H. Kumagai, and W. C. Boncyk (1992), A study of rain estimation methods from space using dual-wavelength radar measurements at near-nadir incidence over ocean, *J. Atmos. Oceanic Technol.*, *9*(4), 364–382, doi:10.1175/1520-0426(1992)009<0364:ASOREM>2.0.CO;2.

Mie, G. (1908), Beiträge zur optik trüber medien, speziell kolloidaler metallösungen, *Annalen der Physik*, *330*(3), 377–445, doi:10.1002/andp.19083300302.

Mishchenko, M. I., and L. D. Travis (1998), Capabilities and limitations of a current FORTRAN implementation of the T-matrix method for randomly oriented, rotationally symmetric scatterers, *J. Quant. Spectrosc. Radiat. Transfer*, *60*(3), 309–324, doi:10.1016/S0022-4073(98)00008-9.

Mitra, S. K. (2002), *Digital Signal Processing: A Computer-based Approach*, McGraw-Hill.

Nakamura, K., and T. Iguchi (2007), Dual-wavelength radar algorithm, in *Measuring Precipitation From Space*, edited by V. Levizzani, P. Bauer, and F. J. Turk, chap. 18, pp. 225–234, Springer, doi:10.1007/978-1-4020-5835-6_18.

Newell, D. A., G. Rait, T. Ta, B. Berdanier, D. Draper, M. Kubitschek, and S. Krimchansky (2010), GPM Microwave Imager design, predicted performance and status, in *IEEE Geoscience and Remote Sensing Symposium, 2010*, pp. 546–549, doi:10.1109/IGARSS.2010.5652098.

Newman, A. J., P. A. Kucera, and L. F. Bliven (2009), Presenting the Snowflake Video Imager (SVI), *J. Atmos. Oceanic Technol.*, *26*, 167–179, doi:10.1175/2008JTECHA1148.1.

Peters, G., B. Fischer, H. Münster, M. Clemens, and A. Wagner (2005), Profiles of raindrop size distributions as retrieved by microrain radars, *J. Appl. Meteor.*, *44*, 1930–1949, doi:10.1175/JAM2316.1.

Peterson, B., and S. Ström (1973), *T* matrix for electromagnetic scattering from an arbitrary number of scatterers and representations of E(3), *Phys. Rev. D*, *8*, 3661–3678, doi:10.1103/PhysRevD.8.3661.

Petty, G. W., and W. Huang (2010), Microwave backscatter and extinction by soft ice spheres and complex snow aggregates, *J. Atmos. Sci.*, *67*(3), 769–787, doi:10.1175/2009JAS3146.1.

Pohjola, H., and J. Koistinen (2002), Diagnostics of vertical reflectivity profiles at the radar sites, in *European Conference on Radar in Meteorology and Hydrology, 2002*, pp. 233–237.

Pruppacher, H. R., and J. D. Klett (1997), *Microphysics of clouds and precipitation*, Springer.

Purcell, E. M., and C. R. Pennypacker (1973), Scattering and absorption of light by nonspherical dielectric grains, *Astrophys. J.*, *186*, 705–714, doi:10.1086/152538.

Randall, D. A., et al. (2007), Climate Models and Their Evaluation, in *Climate Change 2007: The Physical Science Basis. Contribution of Working Group I to the Fourth Assessment Report of the Intergovernmental Panel on Climate Change*, chap. 8, pp. 589–662, Cambridge University Press.

Randeu, W. L., M. Schönhuber, and G. Lammer (2002), Real-time measurements and analyses of precipitation micro-structure and dynamics, in *European Conference on Radar in Meteorology and Hydrology, 2002*, pp. 78–83.

Lord Rayleigh (1871), On the scattering of light by small particles, *Philos. Mag.*, *41*(275), 447–451.

Reiter, C. A. (2005), A local cellular model for snow crystal growth, *Chaos Soliton Fract.*, *23*, 1111–1119, doi:10.1016/j.chaos.2004.06.071.

Rinehart, R. E. (1991), *Radar for Meteorogists*, 2 ed., Knight Printing Company.

Rogers, R. R., and M. K. Yau (1989), *A Short Course in Cloud Physics, 3rd edition*, Butterworth-Heinemann.

Rose, C. R., and V. Chandrasekar (2005), A systems approach to GPM dual-frequency retrieval, *IEEE Trans. Geosci. Remote Sens.*, *43*(8), 1816–1826, doi:10.1109/TGRS.2005.851165.

Ryzhkov, A. V., and D. S. Zrnic (2007), Depolarization in ice crystals and its effect on radar polarimetric measurements, *J. Atmos. Oceanic Technol.*, *24*(7), 1256–1267, doi:10.1175/JTECH2034.1.

Ryzhkov, A. V., S. E. Giangrande, and T. J. Schuur (2005), Rainfall estimation with a polarimetric prototype of WSR-88D, *J. Appl. Meteor.*, *44*(4), 502–515, doi:10.1175/JAM2213.1.

Satoh, S., et al. (2004), Development of spaceborne dual-frequency precipitation radar for the Global Precipitation Measurement, in *24th International Symposium on Space Technology and Science, ISTS*.

Sekhon, R. S., and R. C. Srivastava (1970), Snow size spectra and radar reflectivity, *J. Atmos. Sci.*, *27*(2), 299–307, doi:10.1175/1520-0469(1970)027<0299:SSSARR>2.0.CO;2.

Seliga, T. A., and V. N. Bringi (1976), Potential use of radar differential reflectivity measurements at orthogonal polarizations for measuring precipitation, *J. Appl. Meteor.*, *15*(1), doi:10.1175/1520-0450(1976)015<0069:PUORDR>2.0.CO;2.

Sheppard, B. E. (1990), Measurement of raindrop size distributions using a small Doppler radar, *J. Atmos. Oceanic Technol.*, *7*, 255–268, doi:10.1175/1520-0426(1990)007<0255:MORSDU>2.0.CO;2.

Sihvola, A. H., and J. A. Kong (1988), Effective permittivity of dielectric mixtures, *IEEE Trans. Geosci. Remote Sens.*, *26*(4), 420–429, doi:10.1109/36.3045.

Smith, E., et al. (2007), International Global Precipitation Measurement (GPM) program and mission: An overview, in *Measuring Precipitation From Space*, edited by V. Levizzani, P. Bauer, and F. J. Turk, chap. 48, pp. 611–653, Springer, doi:10.1007/978-1-4020-5835-6_48.

Smith, P. L. (1984), Equivalent radar reflectivity factors for snow and ice particles, *J. Climate Appl. Meteor.*, *23*, 1258–1260, doi:10.1175/1520-0450(1984)023<1258:ERRFFS>2.0.CO;2.

Sorensen, C. M. (2001), Light scattering by fractal aggregates: A review, *Aerosol Sci. Technol.*, *35*, 648–687, doi:10.1080/02786820117868.

Stephens, G. L., et al. (2002), The CloudSat mission and the A-TRAIN - A new dimension of space-based observations of clouds and precipitation, *Bull. Am. Meteorol. Soc.*, *83*(12), 1771–1790, doi:10.1175/BAMS-83-12-1771.

Stephens, G. L., et al. (2008), CloudSat mission: Performance and early science after the first year of operation, *J. Geophys. Res.*, *113*, D00A18, doi:10.1029/2008JD009982.

Stephens, G. L., et al. (2012), An update on Earth's energy balance in light of the latest global observations, *Nature Geosci.*, *5*, 691–696, doi:10.1038/ngeo1580.

Stokes, G. M., and S. E. Schwartz (1994), The Atmospheric Radiation Measurement (ARM) program: Programmatic background and design of the cloud and radiation test bed, *Bull. Amer. Meteor. Soc.*, *75*, 1201–1221, doi:10.1175/1520-0477(1994)075<1201:TARMPP>2.0.CO;2.

Straka, J. M., D. S. Zrnic, and A. V. Ryzhkov (2000), Bulk hydrometeor classification and quantification using polarimetric radar data: Synthesis of relations, *J. Appl. Meteor.*, *39*(8), 1341–1372, doi:10.1175/1520-0426(2001)018<0892:TAPFAC>2.0.CO;2.

Tanelli, S., S. L. Durden, E. Im, K. S. Pak, D. G. Reinke, P. Partain, J. M. Haynes, and R. T. Marchand (2008), CloudSat's Cloud Profiling Radar After Two Years in Orbit: Performance, Calibration, and Processing, *IEEE Trans. Geosci. Remote Sens.*, *46*(11), 3560–3573, doi:10.1109/TGRS.2008.2002030.

Tanelli, S., S. L. Durden, E. Im, G. M. Heymsfield, P. Racette, and D. O. Starr (2009), Next-generation spaceborne cloud profiling radars, in *2009 IEEE Radar Conference*, pp. 1–4, doi:10.1109/RADAR.2009.4977116.

Testud, J., S. Oury, R. A. Black, P. Amayenc, and X. Dou (2001), The Concept of "Normalized" Distribution to Describe Raindrop Spectra: A Tool for Cloud Physics and Cloud Remote Sensing, *J. Appl. Meteor.*, *40*, 1118–1140, doi:10.1175/1520-0450(2001)040<1118:TCONDT>2.0.CO;2.

Thurai, M., and V. N. Bringi (2005), Drop axis ratios from a 2D Video Disdrometer, *J. Atmos. Oceanic Technol.*, *22*(7), 966–978, doi:10.1175/JTECH1767.1.

Thurai, M., and V. N. Bringi (2008), Rain microstructure from polarimetric radar and advanced disdrometers, in *Precipitation: Advances in Measurement, Estimation and Prediction*, edited by S. Michaelides, chap. 10, pp. 231–284, Springer.

Thurai, M., G. J. Huang, V. N. Bringi, W. L. Randeu, and M. Schönhuber (2007), Drop shapes, model comparisons, and calculations of polarimetric radar parameters in rain, *J. Atmos. Oceanic Technol.*, *24*(6), 1019–1032, doi:10.1175/JTECH2051.1.

Thurai, M., V. N. Bringi, M. Szakáll, S. K. Mitra, K. V. Beard, and S. Borrmann (2009), Drop shapes and axis ratio distributions: Comparison between 2d video disdrometer and wind-tunnel measurements, *J. Atmos. Oceanic Technol.*, *26*(7), 1427–1432, doi:10.1175/2009JTECHA1244.1.

Tokay, A., A. Kruger, and W. F. Krajewski (2001), Comparison of drop size distribution measurements by impact and optical disdrometers, *J. Appl. Meteor.*, *40*(11), 2083–2097, doi:10.1175/1520-0450(2001)040<2083:CODSDM>2.0.CO;2.

Tokay, A., D. B. Wolff, K. R. Wolff, and P. Bashor (2003), Rain gauge and disdrometer measurements during the Keys Area Microphysics Project (KAMP), *J. Atmos. Oceanic Technol.*, *20*(11), 1460–1477, doi:10.1175/1520-0426(2003)020<1460:RGADMD>2.0.CO;2.

Tokay, A., P. G. Bashor, and K. R. Wolff (2005), Error characteristics of rainfall measurements by collocated Joss-Waldvogel disdrometers, *J. Atmos. Oceanic Technol.*, *22*(5), 513–527, doi:10.1175/JTECH1734.1.

Tyynelä, J., J. Leinonen, D. Moisseev, and T. Nousiainen (2011), Radar backscattering from snowflakes: comparison of fractal, aggregate and soft-spheroid models, *J. Atmos. Oceanic Technol.*, *28*, 1365–1372, doi:710.1175/JTECH-D-11-00004.1.

Tyynelä, J., J. Leinonen, C. Westbrook, D. Moisseev, and T. Nousiainen (2013), Applicability of the Rayleigh-Gans approximation for scattering by snowflakes at microwave frequencies in vertical incidence, *J. Geophys. Res.*, *118*, doi:10.1002/jgrd.50167.

Ulbrich, C. W. (1983), Natural variations in the analytical form of the raindrop size distribution, *J. Climate Appl. Meteor.*, *22*, 1764–1775, doi:10.1175/1520-0450(1983)022<1764:NVITAF>2.0.CO;2.

van de Hulst, H. C. (1957), *Light Scattering by Small Particles*, John Wiley & Sons.

Vivekanandan, J., V. N. Bringi, M. Hagen, and P. Meischner (1994), Polarimetric radar studies of atmospheric ice particles, *IEEE Trans. Geosci. Remote Sens.*, *32*(1), 1–10, doi:10.1109/36.285183.

Wang, Y., and V. Chandrasekar (2010), Quantitative precipitation estimation in the CASA X-band dual-polarization radar network, *J. Atmos. Oceanic Technol.*, *27*(10), 1665–1676, doi:10.1175/2010JTECHA1419.1.

Waterman, P. C. (1965), Matrix formulation of electromagnetic scattering, *Proc. IEEE*, *53*(8), 805–812, doi:10.1109/PROC.1965.4058.

Westbrook, C., R. C. Ball, and P. R. Field (2006), Radar scattering by aggregate snowflakes, *Quart. J. Roy. Meteor. Soc.*, *132*, 897–914, doi:10.1256/qj.05.82.

Westbrook, C. D., R. C. Ball, P. R. Field, and A. J. Heymsfield (2004), Theory of growth by differential sedimentation, with application to snowflake formation, *Phys. Rev. E*, *70*(2), 021,403, doi:10.1103/PhysRevE.70.021403.

Williams, C. R., A. Kruger, K. S. Gage, A. Tokay, R. Cifelli, W. F. Krajewski, and C. Kummerow (2000), Comparison of simultaneous rain drop size distributions estimated from two surface disdrometers and a UHF profiler, *Geophys. Res. Lett.*, *27*(12), 1763–1766, doi:10.1029/1999GL011100.

Yurkin, M. A., and A. G. Hoekstra (2007), The discrete dipole approximation: an overview and recent developments, *J. Quant. Spectrosc. Radiat. Transfer*, *106*(1), 558–589, doi:10.1016/j.jqsrt.2007.01.034.

Yurkin, M. A., and A. G. Hoekstra (2011), The discrete-dipole-approximation code ADDA: Capabilities and known limitations, *J. Quant. Spectrosc. Radiat. Transfer*, *112*, 2234–2247, doi:10.1016/j.jqsrt.2011.01.031.

Zubko, E., et al. (2010), Validity criteria of the discrete dipole approximation, *Appl. Opt.*, *49*(8), 1267–1279, doi:10.1364/AO.49.001267.

Finnish Meteorological Institute Contributions

1. Joffre, Sylvain M., 1988. Parameterization and assessment of processes affecting the long-range transport of airborne pollutants over the sea. 49 p.

2. Solantie, Reijo, 1990. The climate of Finland in relation to its hydrology, ecology and culture. 130 p.

3. Joffre, Sylvain M. and Lindfors, Virpi, 1990. Observations of airborne pollutants over the Baltic Sea and assessment of their transport, chemistry and deposition. 41 p.

4. Lindfors, Virpi, Joffre, Sylvain M. and Damski, Juhani, 1991. Determination of the wet and dry deposition of sulphur and nitrogen compounds over the Baltic Sea using actual meteorological data. 111 p.

5. Pulkkinen, Tuija, 1992. Magnetic field modelling during dynamic magnetospheric processes. 150 p.

6. Lönnberg, Peter, 1992. Optimization of statistical interpolation. 157 p.

7. Viljanen, Ari, 1992. Geomagnetic induction in a one- or two-dimensional earth due to horizontal ionospheric currents. 136 p.

8. Taalas, Petteri, 1992. On the behaviour of tropospheric and stratospheric ozone in Northern Europe and in Antarctica 1987-90. 88 p.

9. Hongisto, Marke, 1992. A simulation model for the transport, transformation and deposition of oxidized nitrogen compounds in Finland — 1985 and 1988 simulation results. 114 p.

10. Taalas, Petteri, 1993. Factors affecting the behaviour of tropospheric and stratospheric ozone in the European Arctic and Antarctica. 138 s.

11. Mälkki, Anssi, 1993. Studies on linear and non-linear ion waves in the auroral acceleration region. 109 p.

12. Heino, Raino, 1994. Climate in Finland during the period of meteorological observations. 209 p.

13. Janhunen, Pekka, 1994. Numerical simulations of E-region irregularities and ionosphere-magnetosphere coupling. 122 p.

14. Hillamo, Risto E., 1994. Development of inertial impactor size spectroscopy for atmospheric aerosols. 148 p.

15. Pakkanen, Tuomo A., 1995. Size distribution measurements and chemical analysis of aerosol components. 157 p.

16. Kerminen, Veli-Matti, 1995. On the sulfuric acid-water particles via homogeneous nucleation in the lower troposphere. 101 p.

17. Kallio, Esa, 1996. Mars-solar wind interaction: Ion observations and their interpretation. 111 p.

18. Summanen, Tuula, 1996. Interplanetary Lyman alpha measurements as a tool to study solar wind properties. 114 p.

19. Rummukainen, Markku, 1996. Modeling stratospheric chemistry in a global three-dimensional chemical transport model, SCTM-1. Model development. 206 p.

20. Kauristie, Kirsti, 1997. Arc and oval scale studies of auroral precipitation and electrojets during magnetospheric substorms. 134 p.

21. Hongisto, Marke, 1998. Hilatar, A regional scale grid model for the transport of sulphur and nitrogen compounds. 152 p.

22. Lange, Antti A.I., 1999. Statistical calibration of observing systems. 134 p.

23. Pulkkinen, Pentti, 1998. Solar differential rotation and its generators: computational and statistical studies. 108 p.

24. Toivanen, Petri, 1998. Large-scale electromagnetic fields and particle drifts in time-dependent Earth's magnetosphere. 145 p.

25. Venäläinen, Ari, 1998. Aspects of the surface energy balance in the boreal zone. 111 p.

26. Virkkula, Aki, 1999. Field and laboratory studies on the physical and chemical properties of natural and anthropogenic tropospheric aerosol. 178 p.

27. Siili, Tero, 1999. Two-dimensional modelling of thermal terrain-induced mesoscale circulations in Mars' atmosphere. 160 p.

28. Paatero, Jussi, 2000. Deposition of Chernobyl-derived transuranium nuclides and short-lived radon-222 progeny in Finland. 128 p.

29. Jalkanen, Liisa, 2000. Atmospheric inorganic trace contaminants in Finland, especially in the Gulf of Finland area. 106 p.

30. Mäkinen, J. Teemu, T. 2001. SWAN Lyman alpha imager cometary hydrogen coma observations. 134 p.

31. Rinne, Janne, 2001. Application and development of surface layer flux techniques for measurements of volatile organic compound emissions from vegetation. 136 p.

32. Syrjäsuo, Mikko T., 2001. Auroral monitoring system: from all-sky camera system to automated image analysis. 155 p.

33. Karppinen, Ari, 2001. Meteorological pre-processing and atmospheric dispersion modelling of urban air quality and applications in the Helsinki metropolitan area. 94 p.

34. Hakola, Hannele, 2001. Biogenic volatile organic compound (VOC) emissions from boreal deciduous trees and their atmospheric chemistry. 125 p.

35. Merenti-Välimäki, Hanna-Leena, 2002. Study of automated present weather codes.153 p.

36. Tanskanen, Eija I., 2002. Terrestrial substorms as a part of global energy flow. 138 p.

37. Nousiainen, Timo, 2002. Light scattering by nonspherical atmospheric particles. 180 p.

38. Härkönen, Jari, 2002. Regulatory dispersion modelling of traffic-originated pollution. 103 p.

39. Oikarinen, Liisa, 2002. Modeling and data inversion of atmospheric limb scattering measurements. 111 p.

40. Hongisto, Marke, 2003. Modelling of the transport of nitrogen and sulphur contaminants to the Baltic Sea Region. 188 p.

41. Palmroth, Minna, 2003. Solar wind – magnetosphere interaction as determined by observations and a global MHD simulation. 147 p.

42. Pulkkinen, Antti, 2003. Geomagnetic induction during highly disturbed space weather conditions: Studies of ground effects 164 p.

43. Tuomenvirta, Heikki, 2004. Reliable estimation of climatic variations in Finland. 158 p.

44. Ruoho-Airola, Tuija, 2004. Temporal and regional patterns of atmospheric components affecting acidification in Finland. 115 p.

45. Partamies, Noora, 2004. Meso-scale auroral physics from groundbased observations. 122 p.

46. Teinilä, Kimmo, 2004. Size resolved chemistry of particulate ionic compounds at high latitudes. 138 p.

47. Tamminen, Johanna, 2004. Adaptive Markov chain Monte Carlo algorithms with geophysical applications. 156 p.

48. Huttunen, Emilia, 2005. Interplanetary shocks, magnetic clouds, and magnetospheric storms. 142 p.

49. Sofieva, Viktoria, 2005. Inverse problems in stellar occultation. 110 p.

50. Harri, Ari-Matti, 2005. In situ observations of the atmospheres of terrestrial planetary bodies. 246 p.

51. Aurela, Mika, 2005. Carbon dioxide exchange in subarctic ecosystems measured by a micrometeorological technique. 132 p.

52. Damski, Juhani, 2005. A Chemistry-transport model simulation of the stratospheric ozone for 1980 to 2019. 147 p.

53. Tisler, Priit, 2006. Aspects of weather simulation by numerical process. 110 p.

54. Arola, Antti, 2006. On the factors affecting short- and long-term UV variability. 82 p.

55. Verronen, Pekka T., 2006. Ionosphere-atmosphere interaction during solar proton events. 146 p.

56. Hellén, Heidi, 2006. Sources and concentrations of volatile organic compounds in urban air. 134 p.

57. Pohjola, Mia, 2006. Evaluation and modelling of the spatial and temporal variability of particulate matter in urban areas. 143 p.

58. Sillanpää, Markus, 2006. Chemical and source characterisation of size-segregated urban air particulate matter. 184 p.

59. Niemelä, Sami, 2006. On the behaviour of some physical parameterization methods in high resolution numerical weather prediction models. 136 p.

60. Karpechko, Alexey, 2007. Dynamical processes in the stratosphere and upper troposphere and their influence on the distribution of trace gases in the polar atmosphere. 116 p.

61. Eresmaa, Reima, 2007. Exploiting ground-based measurements of Global Positioning System for numerical weather prediction. 95 p.

62. Seppälä, Annika, 2007. Observations of production and transport of NOx formed by energetic particle precipitation in the polar night atmosphere. 100 p.

63. Rontu, Laura, 2007. Studies on orographic effects in a numerical weather prediction model. 151 p.

64. Vajda, Andrea, 2007. Spatial variations of climate and the impact of disturbances on local climate and forest recovery in northern Finland. 139 p.

65. Laitinen, Tiera, 2007. Rekonnektio Maan magnetosfäärissä – Reconnection in Earth's magnetosphere. 226 s.

66. Vanhamäki, Heikki, 2007. Theoretical modeling of ionospheric electrodynamics including induction effects. 170 p.

67. Lindfors. Anders, 2007. Reconstruction of past UV radiation. 123 p.

68. Sillanpää, Ilkka, 2008. Hybrid modelling of Titan's interaction with the magnetosphere of Saturn. 200 p.

69. Laine, Marko, 2008. Adaptive MCMC methods with applications in environmental and geophysical models. 146 p.

70. Tanskanen, Aapo, 2008. Modeling of surface UV radiation using satellite data. 109 p.

71. Leskinen, Ari, 2008. Experimental studies on aerosol physical properties and transformation in environmental chambers. 116 p.

72. Tarvainen, Virpi, 2008. Development of biogenetic VOC emission inventories for the boreal forest. 137 p.

73. Lohila, Annalea, 2008. Carbon dioxide exchange on cultivated and afforested boreal peatlands. 110 p.

74. Saarikoski, Sanna, 2008. Chemical mass closure and source-specific composition of atmospheric particles. 182 p.

75. Pirazzini, Roberta, 2008. Factors controlling the surface energy budget over snow and ice. 141 p.

76. Salonen, Kirsti, 2008. Towards the use of radar winds in numerical weather prediction. 87 p.

77. Luojus, Kari, 2009. Remote sensing of snow-cover for the boreal forest zone using microwave radar. 178 p.

78. Juusola, Liisa, 2009. Observations of the solar wind-magnetosphere-ionosphere coupling. 167 p.

79. Waldén, Jari, 2009. Meteorology of gaseous air pollutants. 177 p.

80. Mäkelä, Jakke, 2009. Electromagnetic signatures of lightning near the HF frequency band. 152 p.

81. Thum, Tea, 2009. Modelling boreal forest CO_2 exchange and seasonality. 140 p.

82. Lallo, Marko, 2010. Hydrogen soil deposition and atmospheric variations in the boreal zone. 91 p.

83. Sandroos, Arto, 2010. Shock acceleration in the solar corona. 116 p.

84. Lappalainen, Hanna, 2010. Role of temperature in the biological activity of a boreal forest. 107 p.

85. Mielonen, Tero, 2010. Evaluation and application of passive and active optical remote sensing methods for the measurement of atmospheric aerosol properties. 125 p.

86. Lakkala, Kaisa, 2010. High quality polar UV measurements : scientific analyses and transfer of the irradiance scale. 156 p.

87. Järvinen, Riku, 2011. On ion escape from Venus. 150 p.

88. Saltikoff, Elena, 2011. On the use of weather radar for mesoscale applications in northern conditions. 120 p.

89. Timonen, Hilkka, 2011. Chemical characterization of urban background aerosol using online and filter methods. 176 p.

90. Hyvärinen, Otto, 2011. Categorical meteorological products : evaluation and analysis. 138 p.

91. Mäkelä, Antti, 2011. Thunderstorm climatology and lightning location applications in northern Europe. 158 p.

92. Hietala, Heli, 2012. Multi-spacecraft studies on space plasma shocks. 132 p.

93. Leinonen, Jussi, 2013. Impact of the microstructure of precipitation and hydrometeors on multi-frequency radar observations. 140 p.